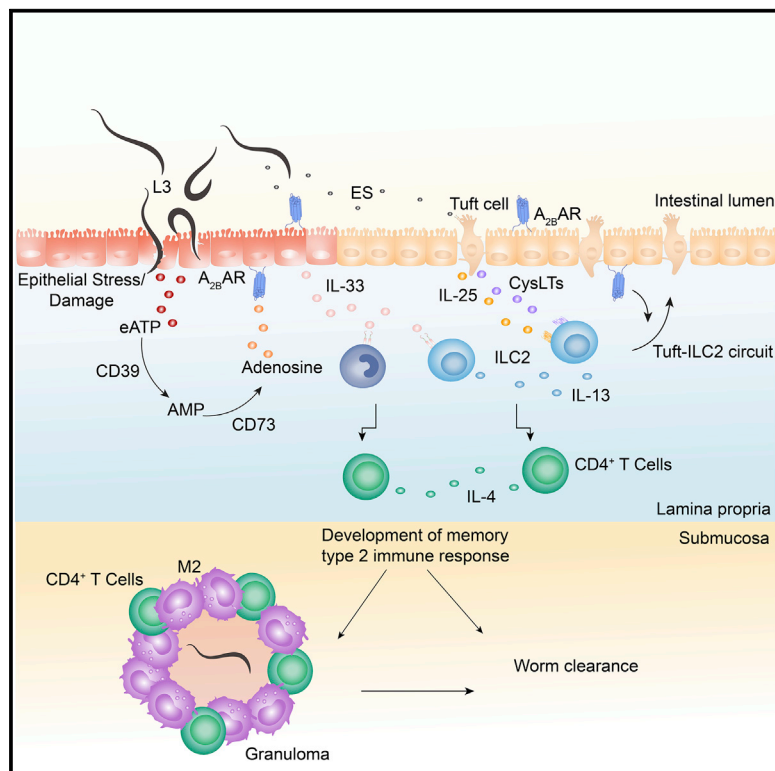**Article**

Adenosine metabolized from extracellular ATP promotes type 2 immunity through triggering A$_{2B}$AR signaling in intestinal epithelial cells

Graphical abstract

Authors

Darine W. El-Naccache, Fei Chen, Mark J. Palma, ..., Karen L. Edelblum, György Haskó, William C. Gause

Correspondence

gh2503@cumc.columbia.edu (G.H.),
gausewc@njms.rutgers.edu (W.C.G.)

In brief

Type 2 immunity mediates allergic inflammation and protective responses to helminths. El-Naccache et al. report in a murine helminth model that adenosine, derived from extracellular ATP, binds the A$_{2B}$ adenosine receptor expressed on intestinal epithelial cells, initiating the type 2 response by promoting IL-33 release and tuft cell hyperplasia.

Highlights

- Adenosine binding A$_{2B}$AR on IECs promotes type 2 immunity to helminths

- This interaction results in increased IL-33 and formation of cleaved bioactive forms

- Adenosine-IEC A$_{2B}$AR signaling is also required for tuft cell hyperplasia

- Adenosine is derived from extracellular ATP through CD39-dependent activity

CellPress

Article

Adenosine metabolized from extracellular ATP promotes type 2 immunity through triggering A$_{2B}$AR signaling in intestinal epithelial cells

Darine W. El-Naccache,[1,2] Fei Chen,[1,2] Mark J. Palma,[1,2] Alexander Lemenze,[1,3] Matthew A. Fischer,[1,3] Wenhui Wu,[1,2] Pankaj K. Mishra,[1,2] Holger K. Eltzschig,[4] Simon C. Robson,[5] Francesco Di Virgilio,[6] George S. Yap,[1,2] Karen L. Edelblum,[1,3] György Haskó,[7,*] and William C. Gause[1,2,8,*]

[1]Center for Immunity and Inflammation, New Jersey Medical School, Rutgers—The State University of New Jersey, Newark, NJ 07101, USA
[2]Department of Medicine, New Jersey Medical School, Rutgers—The State University of New Jersey, Newark, NJ 07101, USA
[3]Department of Pathology, Immunology, and Laboratory Medicine, New Jersey Medical School, Rutgers—The State University of New Jersey, Newark, NJ 07101, USA
[4]Department of Anesthesiology, University of Texas at Houston Medical School, Houston, TX 77030, USA
[5]Center for Inflammation Research, Department of Anesthesia, Critical Care & Pain Medicine and Division of Gastroenterology, Department of Medicine, Beth Israel Deaconess Medical Center, Harvard Medical School, 330 Brookline Avenue, Boston, MA 02215, USA
[6]Department of Medical Sciences, University of Ferrara, Ferrara, Italy
[7]Department of Anesthesiology, Columbia University, New York, NY, USA
[8]Lead contact
*Correspondence: gh2503@cumc.columbia.edu (G.H.), gausewc@njms.rutgers.edu (W.C.G.)
https://doi.org/10.1016/j.celrep.2022.111150

SUMMARY

Intestinal nematode parasites can cross the epithelial barrier, causing tissue damage and release of danger-associated molecular patterns (DAMPs) that may promote host protective type 2 immunity. We investigate whether adenosine binding to the A$_{2B}$ adenosine receptor (A$_{2B}$AR) on intestinal epithelial cells (IECs) plays an important role. Specific blockade of IEC A$_{2B}$AR inhibits the host protective memory response to the enteric helminth, *Heligmosomoides polygyrus bakeri (Hpb)*, including disruption of granuloma development at the host-parasite interface. Memory T cell development is blocked during the primary response, and transcriptional analyses reveal profound impairment of IEC activation. Extracellular ATP is visualized 24 h after inoculation and is shown in CD39-deficient mice to be critical for the adenosine production mediating the initiation of type 2 immunity. Our studies indicate a potent adenosine-mediated IEC pathway that, along with the tuft cell circuit, is critical for the activation of type 2 immunity.

INTRODUCTION

Soil-transmitted helminth infections are a global health issue, with high rates of morbidity and an estimated 1.5 billion people infected worldwide. The incidence of high reinfection rates and increased susceptibility to co-infection with other infectious agents warrants the need for the development of novel, improved treatments, and prevention strategies. Helminth infections and other insults such as allergens and sterile particles can induce a type 2 immune response in humans and experimental mouse models. This response is characterized by the upregulation of interleukin (IL)-4, IL-5, and IL-13 by lymphocytes and myeloid cells, alternatively activated (M2) macrophages and fibrosis (Gause et al., 2020; El-Naccache et al., 2020).

Recent studies have revealed new insights into the initiation and development of the host protective type 2 immune response to enteric helminths. Specialized intestinal epithelial tuft cells sense invading parasites in the lumen, triggering their secretion of cysteinyl leukotrienes, which, in conjunction with their consti-

tutive secretion of IL-25, can promote IL-13 production by activated innate lymphoid cells type 2 (ILC2s). IL-13 stimulates tuft cell hyperplasia, triggering a tuft cell-ILC2 circuit (Mcginty et al., 2020; Faniyi et al., 2020; Schneider et al., 2018). However, other studies have also shown a major role for IL-33 (Roan et al., 2019; Liew et al., 2016; Ryan et al., 2020; Shimokawa et al., 2017; Humphreys et al., 2008), while others indicate a more minor contribution (Zaiss et al., 2013), suggesting that there are likely multiple pathways contributing to helminth-induced type 2 immunity (Vannella et al., 2016; Mcginty et al., 2020; Gause et al., 2020).

Adenosine can play an important role in type 2 immunity to helminth infections (Csoka et al., 2018a; Patel et al., 2014). Adenosine is a purine nucleoside that can regulate various biological processes by binding to the G protein-coupled cell surface adenosine receptors (A$_1$, A$_{2A}$, A$_{2B}$, and A$_3$AR). The accumulation of extracellular adenosine can be due to its release from cells or the release of ATP followed by its catabolism to adenosine by cell surface ecto-nucleotidases CD39 and CD73 (Heine et al., 2001; Knapp et al.,

2012; Strater, 2006). Recent studies have demonstrated that the A$_{2B}$ adenosine receptor (A$_{2B}$AR) can modulate type 2 immunity. A$_{2B}$AR signaling on macrophages promotes an alternatively activated (M2) phenotype (Csoka et al., 2012), and A$_{2B}$AR signaling in mast cells induces IL-4 secretion (Ryzhov et al., 2004). $A_{2B}AR^{-/-}$ mice have delayed helminth expulsion and an impaired type 2 immune response (Patel et al., 2014). However, the cell types expressing A$_{2B}$AR receptors that participate in this initiation, whether extracellular ATP (eATP) contributes to the adenosine-A$_{2B}$AR axis, and whether A$_{2B}$AR signaling is required for memory T cell development, remain unknown.
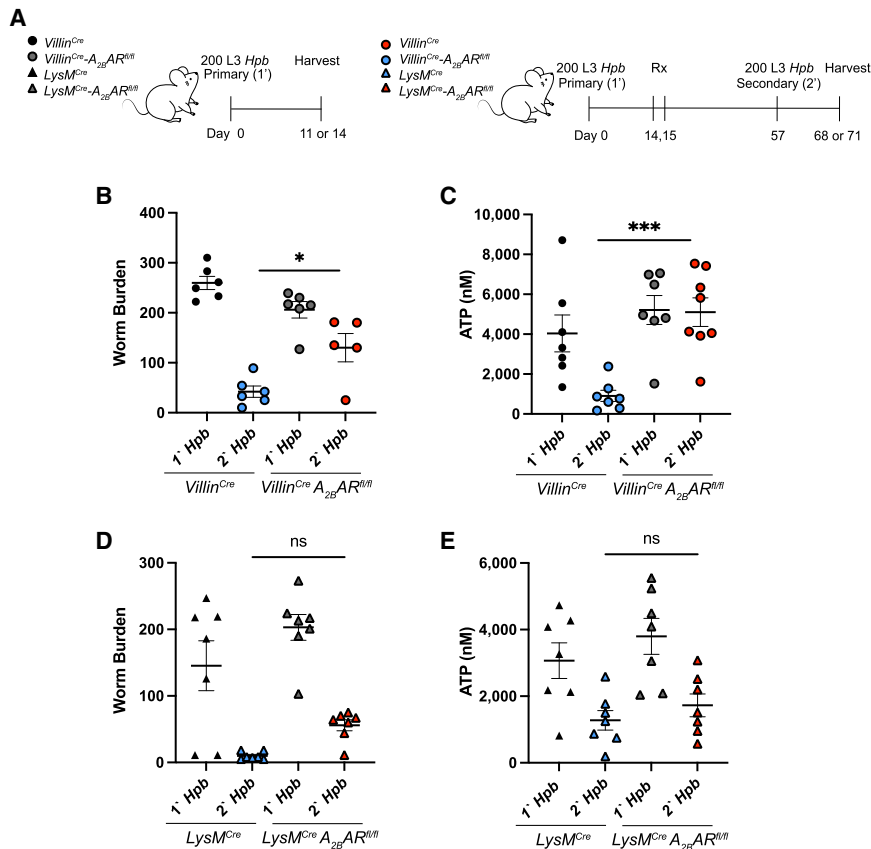
The murine intestinal nematode parasite *Heligmosomoides polygyrus bakeri (Hpb)* is an established experimental model used to study the initiation of type 2 immunity and the subsequent CD4 T cell-dependent memory type 2 immune response (Reynolds et al., 2012; Anthony et al., 2006, 2007). Here, we report that A$_{2B}$AR expression by intestinal epithelial cells (IECs), but not myeloid cells, is essential for an effective memory response after *Hpb* inoculation. We further show that A$_{2B}$AR IEC signaling mediates the development of memory T cells during the primary response but is not required for subsequent memory T cell activation after secondary inoculation. During the primary response, increased bioactive IL-33 and initiation of type 2 immunity was dependent on IEC A$_{2B}$AR signaling as early as 24 h after inoculation and triggered marked localized increases in eATP production. Blockade of the ectonucleotidase CD39 similarly inhibited memory type 2 immune responses, indicating the importance of eATP as a catabolic source of extracellular adenosine. These studies reveal a pathway for the initiation of type 2 immunity involving eATP metabolized to adenosine and specifically binding A$_{2B}$AR on IECs.

RESULTS

Intestinal epithelial A$_{2B}$AR signaling promotes host protective memory immune response to intestinal helminth *Hpb*

Hpb is a strictly enteric murine intestinal nematode parasite that triggers a potent and polarized type 2 immune response. After peroral inoculation, larval parasites invade intestinal tissues residing in the submucosa for 8 days. They then return as adults to the intestinal lumen, where they persist for prolonged periods, mating and producing eggs passed in the feces. Secondary inoculation after drug-induced worm clearance triggers a potent memory CD4 T cell-dependent type 2 response that mediates effective worm clearance (Reynolds et al., 2012; Anthony et al., 2006). We have previously reported that mice deficient in the A$_{2B}$AR have an impaired type 2 memory immune response and delayed worm expulsion following secondary inoculation (Patel et al., 2014). IECs (Strohmeier et al., 1995; Frick et al., 2009; Hart et al., 2009) and innate immune cells, in particular, macrophages (Xaus et al., 1999), express A$_{2B}$AR. Previous studies have suggested that A$_{2B}$AR signaling drives the differentiation of alternatively activated (M2) macrophages (Csoka et al., 2012, 2014; Koscso et al., 2013), which in turn mediate helminth expulsion during a memory type 2 immune response (Anthony et al., 2006). To examine whether A$_{2B}$AR signaling in macrophages or epithelial cells played a significant role in the host protective

memory response to *Hpb*, we used mice genetically deficient in A$_{2B}$AR in either intestinal epithelial cells (*Villin^{Cre}-A$_{2B}$AR^{fl/fl}*) (Aherne et al., 2015) or myeloid cells (*LysM^{Cre}-A$_{2B}$AR^{fl/fl}*) (Seo et al., 2015). Specifically, mice were inoculated orally with 200 L3 *Hpb* (1'*Hpb*), and 14 days post-infection, mice were administered the anti-helminthic drug pyrantel pamoate via oral gavage for 2 consecutive days, effectively removing all parasites from the gut, as described previously (Anthony et al., 2006). Six weeks post-clearance, A$_{2B}$AR lineage-specific knockout (KO) and control lineage-specific Cre mice were challenged with a secondary inoculation of 200 L3 (2' *Hpb*). At this same time point, control groups of naive A$_{2B}$AR lineage-specific and control Cre mice were given a primary *Hpb* inoculation. Fourteen days later, all of the groups were analyzed for worm burden, and on day 11, the effects on parasite metabolic activity were analyzed (Figure 1A). As shown in Figure 1B, although worm burden was markedly reduced after the secondary inoculation of *Villin^{Cre}* mice, *Villin^{Cre}-A$_{2B}$AR^{fl/fl}* mice administered a secondary inoculation showed significant increases in worm burden, not significantly different from *Villin^{Cre}-A$_{2B}$AR^{fl/fl}* mice given a primary inoculation only, indicating that the memory response was compromised. Although parasites are largely expulsed by day 14 in *Villin^{Cre}* mice after a secondary inoculation, at day 11, surviving larvae have only recently migrated back to the lumen after developing into adult worms during their tissue-dwelling phase in the submucosa and are thus readily detectable. In a separate experiment involving the same treatment groups as in Figure 1B, parasites were collected from the small intestine on day 11 after inoculation. Five adult worms in each treatment group were analyzed for overall metabolic activity by assessing parasite ATP concentration levels, as previously described (Herbert et al., 2009). As shown in Figure 1C, parasite ATP concentrations were significantly reduced in *Villin^{Cre}* mice after secondary inoculation compared to *Villin^{Cre}* mice receiving only a primary inoculation. In marked contrast, parasite ATP concentration levels were not reduced in *Villin^{Cre}-A$_{2B}$AR^{fl/fl}* mice after secondary inoculation (compared to primary inoculation) and were significantly increased over *Villin^{Cre}* mice administered a secondary *Hpb* inoculation. *LysM^{Cre}-A$_{2B}$AR^{fl/fl}* mice, in which A$_{2B}$AR is deleted in myeloid cells, were similarly assessed for host-protective responses following *Hpb* inoculation. As shown in Figure 1D, worm burden was markedly reduced in both *LysM^{Cre}* and *LysM^{Cre}-A$_{2B}$AR^{fl/fl}* mice after secondary inoculation (compared to primary inoculation), as was the fitness of the worms assessed by ATP concentration levels (Figure 1E), suggesting a strong polarized T helper 2 cell (Th2) response. Worm burden experiments in lineage-specific KO mice were repeated with similar results (Figure S2A). To assess whether type 2 responses were generally refractory to the deletion of A$_{2B}$ARs on macrophages, effects on a previously established peritoneal type 2 immune response to sterile inert microparticles (MPs) (Mishra et al., 2019) were examined. Mice were inoculated in the peritoneal cavity with MPs, triggering myeloid cell infiltration and potent elevations in type 2 cytokines, as previously described (Mishra et al., 2019). As shown in Figure S1, at 48 h after inoculation, pronounced elevations in type 2 cytokines and increases in M2 macrophages were blocked in MP-inoculated *LysM^{Cre}-A$_{2B}$AR^{fl/fl}* mice compared to inoculated *LysM^{Cre}* mice in this experimental

A

B **C**

D **E**

model of sterile inflammation. Taken together, our data thus demonstrate a key role for IEC-specific A$_{2B}$AR signaling in the protective type 2 memory mucosal immune response to the intestinal helminth, *Hpb*. In contrast, in a non-barrier tissue microenvironment, A$_{2B}$AR signaling in myeloid cells is essential.

Intestinal epithelial A$_{2B}$AR signaling promotes protective memory type 2 immune response at the host-parasite interface
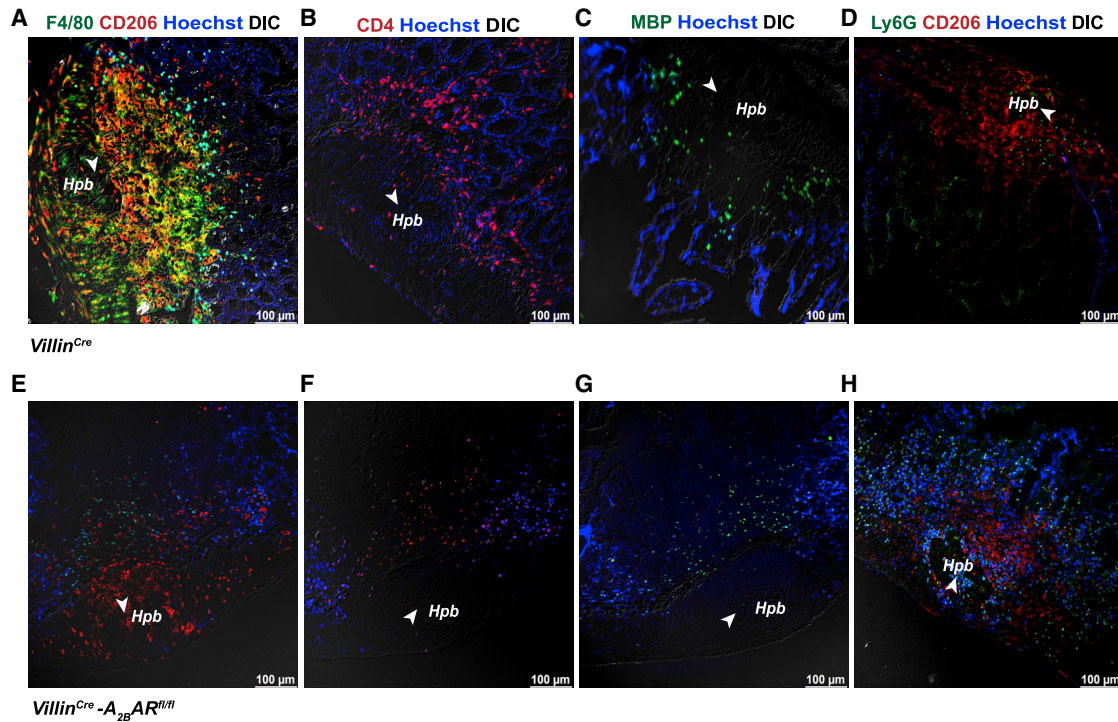
CD4$^+$ T cells and M2 macrophages rapidly accumulate at the host-parasite interface after secondary inoculation, resulting in a distinct granulomatous structure surrounding the tissue-dwelling larvae by day 4 after secondary inoculation, which is critical for the impaired worm development and accelerated expulsion associated with the memory response (Anthony et al., 2006; Morimoto et al., 2004). The increased metabolic activity observed in luminal worms shortly after their migration back to the lumen in *Villin^{Cre}*-A$_{2B}$AR$^{fl/fl}$ mice (Figure 1C) raised the possibility of the impaired formation of the type 2 granuloma. To directly examine whether granulomatous development occurring during the memory type 2 response was affected by A$_{2B}$AR deficiency in IECs, *Villin^{Cre}*-A$_{2B}$AR$^{fl/fl}$ and *Villin^{Cre}* control mice were administered a primary and secondary inoculation of *Hpb*, as described above. On day 4, after secondary inoculation, small intestines were collected, and Swiss-roll cryosections were stained for F4/80 and CD206 to detect M2 macrophages, CD4 for T cells, major basic protein (MBP) for eo-

sinophils, and Ly6G to detect neutrophils. H&E stains showed increased inflammation and granuloma formation in *Villin^{Cre}* compared to *Villin^{Cre}*-A$_{2B}$AR$^{fl/fl}$ mice (Figures S2B and S2C). Furthermore, the granulomas in *Villin^{Cre}*-A$_{2B}$AR$^{fl/fl}$ mice were significantly smaller compared to control *Villin^{Cre}* mice (Figures S2B–S2D). As shown in Figures 2A and S2E, immunofluorescent imaging of the granuloma showed dual-stained M2 macrophages already accumulating around the parasite in granulomas from *Villin^{Cre}* mice, consistent with previous studies (Anthony et al., 2006). In marked contrast, in *Villin^{Cre}*-A$_{2B}$AR$^{fl/fl}$ mice (Figures 2E and S2F), although F4/80$^+$ macrophages were readily detected, their expression of CD206 was markedly reduced, indicating an essential role for IEC A$_{2B}$AR signaling in the recruitment of M2 macrophages within the granuloma. Mean fluorescent intensity of single-color F4/80 and CD206 channels (Figures S2E and S2F) were quantitated. They showed significantly decreased CD206 expression in cells expressing F4/80 in *Hpb*-infected *Villin^{Cre}*-A$_{2B}$AR$^{fl/fl}$ mice compared to *Villin^{Cre}* controls (Figures S2G and S2H). CD4$^+$ T cells were also markedly reduced, suggesting an impairment of peripheral CD4$^+$ T cell activation and migration (Figures 2B and 2F). In contrast, eosinophils and neutrophils showed little differences in their accumulation (Figures 2C, 2D, 2G, and 2H). Gene expression analysis of punch biopsies of granulomas showed significant decreases in M2 markers *Retnla* and *Arg1* 4 days after *Hpb* inoculation (Figures S2I and S2J). IEC A$_{2B}$AR signaling blockade during primary and secondary responses thus impaired granuloma development during the CD4 T cell-dependent memory response.

Memory IL-4 producing CD4 T cells mediate protective immunity in naive mice

Previous studies have shown that the memory type 2 immune response to *Hpb* is IL-4 dependent (Finkelman et al., 1997;

A F4/80 CD206 Hoechst DIC **B** CD4 Hoechst DIC **C** MBP Hoechst DIC **D** Ly6G CD206 Hoechst DIC

Villin^{Cre}

Villin^{Cre}-A_{2B}AR^{fl/fl}

Figure 2. IEC A_{2B}AR signaling promotes recruitment of CD4⁺ T cells and alternatively activated (M2) macrophages required to mediate resistance at the host-parasite interface
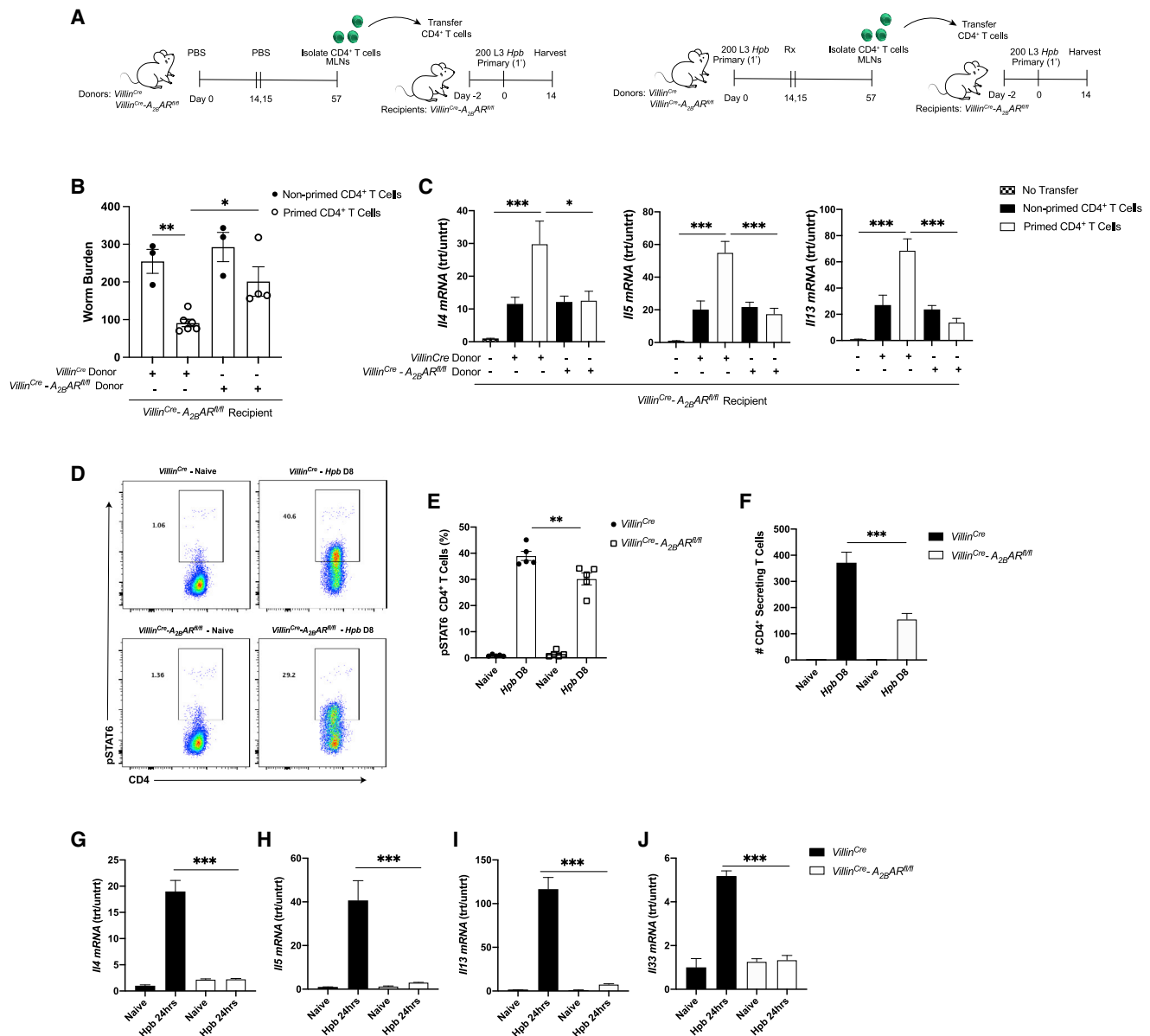
Control *Villin^{Cre}* (A–D) and *Villin^{Cre}-A_{2B}AR^{fl/fl}* (F–H) mice were orally inoculated with 200 L3 *Hpb*, and 14 days later, mice were treated with an anti-helminthic drug, pyrantel pamoate. At 6 weeks post-clearance, mice were challenged with a 2′ *Hpb* inoculation. On day 4 post-2′ inoculation, small intestines were collected. Frozen Swiss-roll sections, 4 μm, stained with Alexa Fluor (AF) 488-F4/80 for macrophages (green), AF647-CD206 for M2 (red) (A and E), AF647-CD4 for T cells (red) (B and F), AF488-MBP for eosinophils (green) (C and G), AF647-CD206 (red), AF488-Ly6G (green) for neutrophils (D and H), and Hoechst 33342 (blue). Arrows, *Hpb*. Scale bar, 100 μm. Figures are representative of 5 individual mice per group. Experiments were repeated at least 2 times with similar results.

Urban et al., 1991), a finding that we confirmed (Figure S3A). Furthermore, adoptive transfer of *in vivo* primed CD4 T cells to naive mice can drive accelerated resistance similar to an intact memory response (Anthony et al., 2006). To corroborate and extend these studies, *wild-type* (*WT*) and *IL-4^{−/−}* mice were infected with *Hpb* and treated with pyrantel pamoate on day 14 after inoculation. Six weeks after primary inoculation, 5 × 10⁶ CD4⁺ T cells, collected from mesenteric lymph nodes (MLNs) and spleen, were transferred to naive recipient mice. Two days later, recipients were inoculated with *Hpb*, and 14 days later, the worm burden was assessed. *WT* and *IL-4^{−/−}* mice that received CD4⁺ T cells from primed *WT* mice had a significant decrease in worm burden at day 14, but *WT* and *IL-4^{−/−}* mice that received CD4 T cells from primed *IL-4^{−/−}* mice had an impairment in worm expulsion and exhibited high worm burden (Figure S3B). These studies indicate that memory effector T cells require IL-4 for their development, but, after their formation, can mediate resistance in the absence of a non-T cell IL-4 source.

A_{2B}AR deficiency in IECs impairs memory CD4⁺ T cell development but not subsequent activation

Our establishment of the memory T cell transfer model provides a basis for further elucidating the role of A_{2B}AR in the development of the type 2 memory response. Our findings indicated

that the T cell-dependent memory response was impaired in *Hpb*-inoculated mice deficient in IEC A_{2B}AR. However, it remained unclear whether inhibition of the response was due to (1) inhibition of initial memory T cell development during priming or (2) impaired subsequent activation of already formed memory T cells following secondary inoculation. To investigate this, *Villin^{Cre}* and *Villin^{Cre}-A_{2B}AR^{fl/fl}* mice were inoculated with *Hpb*, and 14 days later, the drug cleared. Six weeks after drug treatment, 5 × 10⁶ CD4⁺ T cells were isolated from the MLNs and spleen from both treatment groups and transferred to naive recipient *Villin^{Cre}-A_{2B}AR^{fl/fl}* mice. Two days after transfer, recipient mice were inoculated with *Hpb*, and 14 days after the primary *Hpb* inoculation, worm expulsion was assessed (Figure 3A). As shown in Figure 3B, recipient *Villin^{Cre}-A_{2B}AR^{fl/fl}* mice with *Hpb*-primed CD4⁺ T cells from *Villin^{Cre}* control mice experienced significant decreases in worm burden, which was comparable to *WT* control recipient mice with *Hpb*-primed CD4⁺ T cells from *WT* control mice (Figure S3B). In contrast, *Villin^{Cre}-A_{2B}AR^{fl/fl}* mice receiving primed CD4⁺ T cells from *Villin^{Cre}-A_{2B}AR^{fl/fl}* mice showed significant increases in worm burden, not significantly different from increased worm counts in *Villin^{Cre}-A_{2B}AR^{fl/fl}* mice receiving CD4⁺ T cell from uninfected mice (Figure 3B). These findings indicate that the development of CD4 memory Th2 cells during a primary response to helminth

Figure 3. A$_{2B}$AR deficiency in IECs impairs memory CD4$^+$ T cell development and initiation of type 2 response after primary *Hpb* inoculation

Villin^{Cre}-A$_{2B}$AR$^{fl/fl}$ and *Villin^{Cre}* control mice were orally inoculated with 200 L3 *Hpb*, and 14 days later, mice were treated with pyrantel pamoate to expulse parasites. Six weeks post-clearance, CD4$^+$ T cells were magnetically sorted from mesenteric lymph nodes (MLNs) and spleens. Then, 5 × 10^6 CD4$^+$ T cells from both donor treatment groups were transferred to naive *Villin^{Cre}-A$_{2B}$AR$^{fl/fl}$* recipient mice. Controls included CD4$^+$ T cells from naive *Villin^{Cre}-A$_{2B}$AR$^{fl/fl}$* and *Villin^{Cre}* mice injected into naive *Villin^{Cre}-A$_{2B}$AR$^{fl/fl}$* recipient mice. Two days post-transfer, mice were inoculated with 200 L3 *Hpb* (A); 14 days post-infection, worm burden was assessed (B), and small intestine tissues (C) were analyzed by qPCR.

(D–F) Naive *Villin^{Cre}-A$_{2B}$AR$^{fl/fl}$* and control *Villin^{Cre}* mice were given a primary inoculation with 200 L3 *Hpb* for 8 days, and controls included naive mice orally gavaged with PBS. Representative flow cytometric analyses of CD4$^+$ T cells expressing intracellular phosphorylated STAT6 (D) and the mean percentage of CD4$^+$ T cells representing pSTAT6 (E) are shown from MLNs.

(F) MLN CD4$^+$ T cells from pooled mice were sorted, and the number of IL-4-secreting CD4$^+$ T cells determined by ELISpot is shown with technical replicates.

(G–J) *Villin^{Cre}-A$_{2B}$AR$^{fl/fl}$* mice and *Villin^{Cre}* controls were inoculated with 200 L3 *Hpb* for 24 h. Small intestinal tissue was analyzed by qPCR. Data from both experiments show the means and SEMs from 4–6 individual mice per group and are representative of at least 2 independent experiments (1-way ANOVA, multiple comparisons; *p < 0.05, **p < 0.01, ***p < 0.001).

infection requires A$_{2B}$AR signaling in IECs. However, our findings that primed CD4$^+$ T cells from *Villin^{Cre}* WT mice transferred to *Villin^{Cre}-A$_{2B}$AR$^{fl/fl}$* naive mice could effectively mediate worm

expulsion indicate that once CD4$^+$ T memory cells have developed, A$_{2B}$AR signaling on IECs is not required for their subsequent activation and the associated development of a host

protective response. Consistent with the worm expulsion data, gene expression of small intestine type 2 cytokines *Il-4*, *Il-5* and *Il-13* were significantly increased in *Villin^Cre-A_{2B}AR^{fl/fl}* mice receiving primed CD4$^+$ T cells from *Villin^Cre* WT mice but not primed CD4$^+$ T cells from *Villin^Cre-A_{2B}AR^{fl/fl}* mice (Figure 3C). These studies indicate that the development of the memory T cell compartment during a primary response requires A$_{2B}$AR signaling on IECs, but that IEC A$_{2B}$AR signaling is not required for subsequent memory T cell activation.

A$_{2B}$AR deficiency in IECs impaired IL-4R signaling in MLN CD4$^+$ T cells after primary Hpb inoculation

Our finding that memory T cell development is impaired during the primary type 2 immune response to *Hpb* raised the possibility that the primary type 2 response and the associated development of CD4$^+$ T effector cells were inhibited during priming. CD4$^+$ T cell signal transducer and activator of transcription 6 (STAT6) phosphorylation in the MLN is markedly elevated after *Hpb* infection, consistent with increased localized bioavailability of IL-4 (Perona-Wright et al., 2010; Patel et al., 2014). STAT6 phosphorylation was analyzed by flow cytometry on CD4 T cells in *Villin^Cre-A_{2B}AR^{fl/fl}* and *Villin^Cre* mice on day 8 after primary *Hpb* inoculation. As shown in Figures 3D and 3E, significantly decreased STAT6 phosphorylation in CD4$^+$ T cells was observed in *Hpb*-infected *Villin^Cre-A_{2B}AR^{fl/fl}* compared to Villin^Cre mice. Furthermore, IL-4 protein secreted from sorted CD4$^+$ T cells was also significantly reduced in infected *Villin^Cre-A_{2B}AR^{fl/fl}* mice compared to infected *Villin^Cre* control mice at day 8 after primary *Hpb* inoculation, as determined by ELISpot (Figure 3F). Similarly, CD4$^+$ T cell pSTAT6 was also decreased as late as day 11 after both primary and secondary *Hpb* inoculation (Figures S3C and S3D). However, it should be noted that although clearly decreased, there was still significant CD4 effector T cell activity at these later stages of the response. Taken together, these studies indicate that A$_{2B}$AR signaling in epithelial cells is also required for optimal Th2 effector cell development after primary inoculation, but that memory T cell formation is preferentially inhibited.

Epithelial cell A$_{2B}$AR signaling is required during the initiation stages of Hpb primary infection

Our findings suggested a critical role for A$_{2B}$AR signaling in the development of memory T cells following initial infection. *Hpb* can penetrate the epithelial barrier of the small intestine within hours after inoculation and induce type 2 cytokines and likely other as-yet-unidentified signaling pathways (Svetic et al., 1993; Gause et al., 2020). To address the role of epithelial cell A$_{2B}$AR signaling in initiating the early intestinal response, *Villin^Cre-A_{2B}AR^{fl/fl}* mice and corresponding *Villin^Cre* controls were inoculated with *Hpb*, and 24 h later small intestine was collected and RNA isolated for qPCR analyses. Consistent with previous studies, *Hpb*-inoculated *Villin^Cre* mice had a significant increase in the type 2 cytokines *Il-4*, *Il-5, and Il-13*, and the cytokine alarmin *Il33* in intestinal tissues. However, increases in these cytokines were abrogated in *Hpb*-inoculated *Villin^Cre-A_{2B}AR^{fl/fl}* mice (Figures 3G–3J). Cytokines associated with type 1 immunity were also assessed for possible deviation of the response, but increases in *Ifnγ* and *Tnfα* were not markedly different in

Villin^Cre and *Villin^Cre-A_{2B}AR^{fl/fl}* mice at 24 h after *Hpb* inoculation (Figures S4A–S4D).

The profound decrease in the activation of type 2-associated cytokine responses at 24 h after *Hpb* inoculation in *Villin^Cre-A_{2B}AR^{fl/fl}* mice suggested that adenosine signaling on epithelial cells was critical at the initiation of type 2 immunity. To assess changes in IEC activation, small-intestine IECs (DAPI$^-$ CD45$^-$ epithelial cellular adhesion molecule positive [EpCAM$^+$]) were isolated as previously described (Yu et al., 2018; Haber et al., 2017) and sorted from untreated naive *Villin^Cre* mice or *Villin^Cre-A_{2B}AR^{fl/fl}* mice at 24 h after *Hpb* inoculation. Highly purified RNA was individually isolated from 4 mice/treatment groups and then subjected to RNA sequencing (RNA-seq) analyses. Euclidean distance matrix along with hierarchical clustering (Figure 4A) and principal-component analysis (PCA) (Figure 4B) of total transcriptomes from each sample showed similar gene expression profiles of both naive *Villin^Cre* and *Villin^Cre-A_{2B}AR^{fl/fl}* strains. Although some divergence is seen in the PCA plot between *Villin^Cre* and *Villin^Cre-A_{2B}AR^{fl/fl}* naive mice, only 48 genes were differentially expressed ($p_{adj} < 0.05$), with 28 upregulated genes ($p_{adj} < 0.05$, log$_2$fold change [FC] > 0) and 20 downregulated genes ($p_{adj} < 0.05$, log$_2$FC < 0) (Table S1). Pathway enrichment analysis yielded no significant results, and no significant differences in canonical pathways were identified using Ingenuity Pathway Analysis (IPA) analysis. Overall, these analyses indicate that the expression of A$_{2B}$AR, several calcium ion-binding genes, and G protein-coupled receptors are the main differences between the two untreated strains of mice. Thus, under homeostatic conditions in SPF housing, the absence of IEC A$_{2B}$AR signaling did not markedly alter IEC activity. However, after *Hpb* inoculation, *Villin^Cre* and *Villin^cre-A_{2B}AR^{fl/fl}* mice showed distinct gene expression profiles. Volcano plots (Figure 4C) showed a marked reduction in upregulated gene expression in *Villin^Cre A_{2B}AR^{fl/fl}* compared to Villin^Cre after *Hpb* inoculation. A hierarchical clustering heatmap of the significantly differentially expressed genes between *Hpb* inoculated *Villin^Cre-A_{2B}AR^{fl/fl}* and *Hpb*-inoculated control *Villin^Cre* mice showed marked differences between the two groups (Figure S4E). Venn diagram analyses (Figure 4D) depicted the number of upregulated and downregulated genes with a shared and unique expression from *Hpb*-inoculated *Villin^Cre-A_{2B}AR^{fl/fl}* and control *Villin^Cre* mice. Relative to naive mice, 242 genes were differentially expressed in *Hpb*-inoculated Villin^Cre mice with 60% upregulated, while 68 genes were differentially expressed in *Hpb*-inoculated *Villin^Cre-A_{2B}AR^{fl/fl}* mice with 19% upregulated (Table S2). Functional characterization of biological processes and pathways among differentially expressed genes was determined by enrichment IPA (Figure 4E). Gα$_s$/Gα$_q$ and phospholipase C (PLC) signaling, which are known to be activated by A$_{2B}$ARs, were upregulated in *Villin^Cre* but not in *Villin^Cre-A_{2B}AR^{fl/fl}* after *Hpb* inoculation (Figures 4E and 4F). Consistent with effective A$_{2B}$AR deletion, A$_{2B}$AR was not detected in naive or *Hpb*-inoculated *Villin^Cre-A_{2B}AR^{fl/fl}* mice (Figure 4F). We further observed the expression of genes associated with oxidative phosphorylation (OXPHOS) significantly upregulated in IECs of *Villin^Cre* but not *Villin^Cre-A_{2B}AR^{fl/fl}* after *Hpb* inoculation (Figure 4E). OXPHOS is an energy-producing metabolic pathway that contributes to maintaining the intestinal barrier homeostasis (Rath et al.,
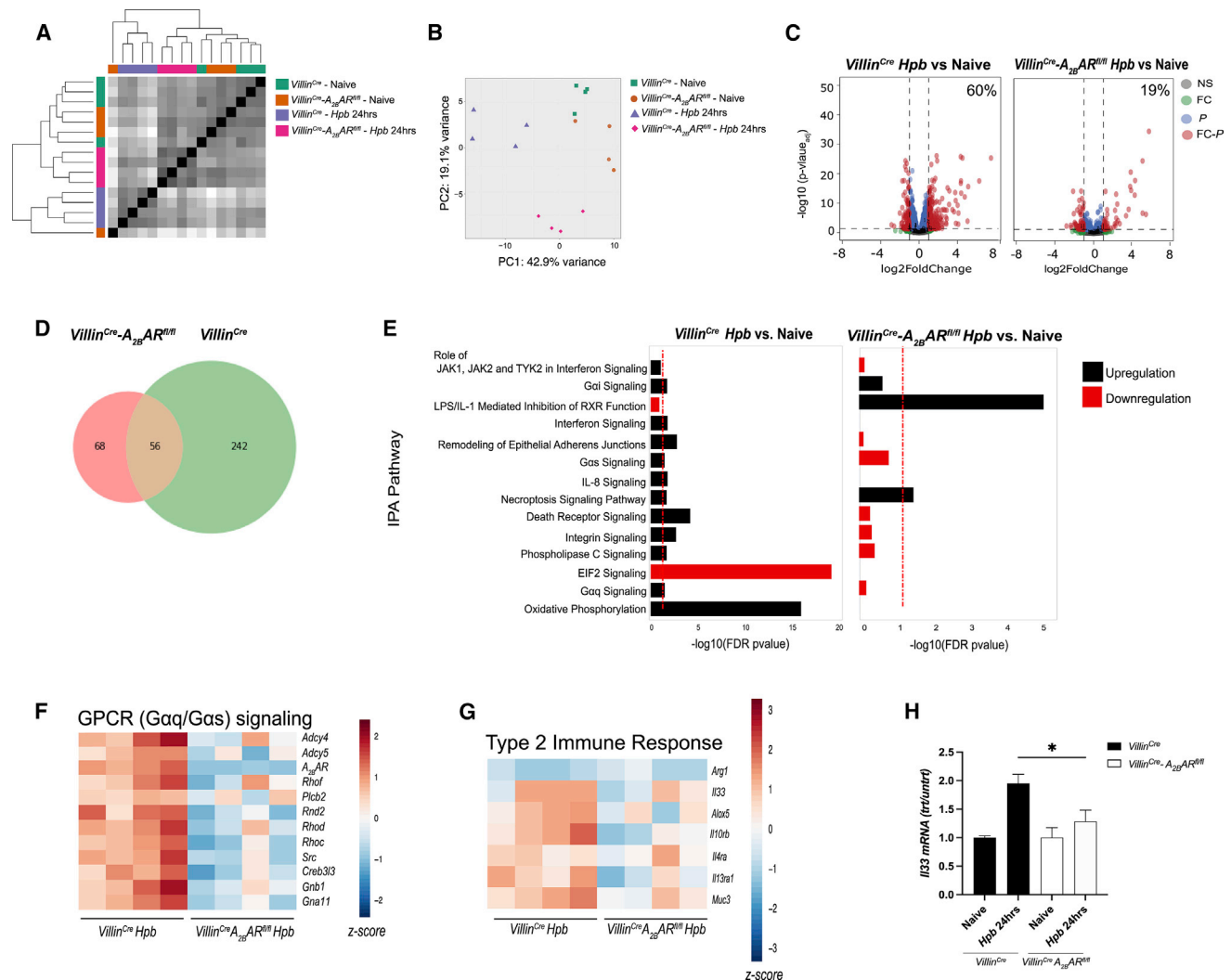
Figure 4. A$_{2B}$AR signaling in IECs is required for their activation at the initiation of the primary response to *Hpb*

(A–E) *Villin^{Cre}-A$_{2B}$AR$^{fl/fl}$* and corresponding control *Villin^{Cre}* mice were orally inoculated with 200 *Hpb* L3; controls included naive mice orally gavaged with PBS. At 24 h after *Hpb* inoculation, IECs were sort purified, RNA was extracted, and RNA-seq was performed. Analyses included a heatmap representing the Euclidean distance matrix of the total transcriptome of each sample, along with hierarchical clustering (A); principal-component analysis (PCA) of the total transcriptome of each sample (B); and volcano plots (C); Venn diagram depicting the number of upregulated and downregulated genes with a shared and unique expression from *Villin^{Cre}-A$_{2B}$AR$^{fl/fl}$* and corresponding controls *Villin^{Cre}* mice relative to naive (D); regulated gene pathways and processes as determined by enrichment Ingenuity Pathway Analysis (IPA) (E).

(F and G) Further analyses revealed heatmaps representing G protein-coupled receptor signaling (F) and type 2 immune response genes (G).
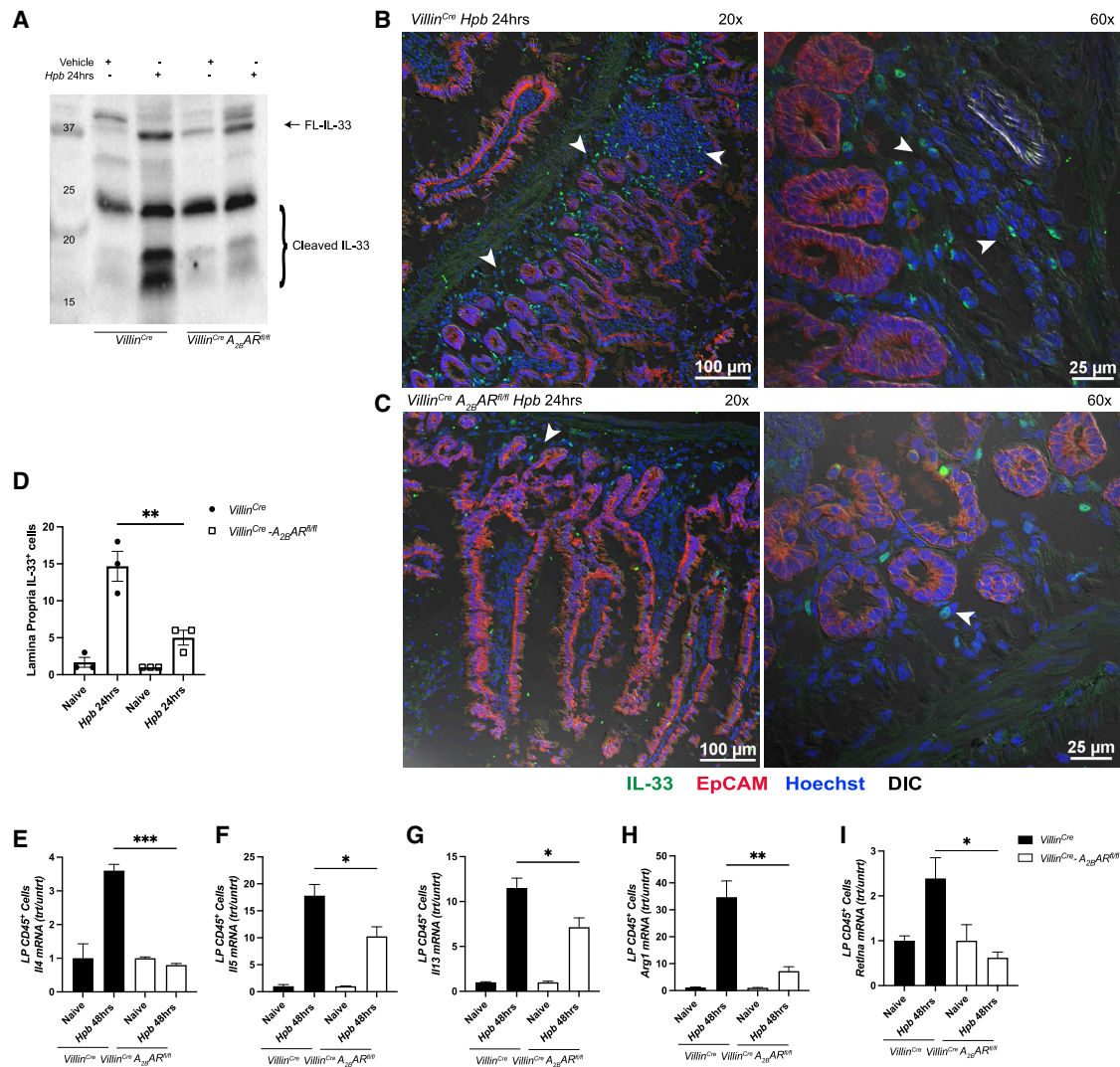
(H) *Villin^{Cre}-A$_{2B}$AR$^{fl/fl}$* mice and *Villin^{Cre}* controls were inoculated with 200 L3 *Hpb* for 24 h. RNA from sorted IECs (EpCAM$^+$CD45$^−$DAPI$^−$) was extracted and analyzed for gene expression of *Il33* by qPCR. Data shown are the means and SEMs from 4 individual mice per group. qPCR experiment shows the means and SEMs from 4–6 individual mice per group and are representative of at least 2 independent experiments (1-way ANOVA, multiple comparisons; *p < 0.05).

2018). This increase in IECs suggests the involvement of the A$_{2B}$AR in regulating the barrier function during the intestinal stress response in helminth infections. Furthermore, type 2 immune response genes and IL-33 were significantly reduced in infected *Villin^{Cre}-A$_{2B}$AR$^{fl/fl}$* compared to infected *Villin^{Cre}* mice (Figure 4G).

To further examine IL-33 expression, in a separate experiment, we performed *Il33* qPCR on IEC mRNA from *Villin^{Cre}* and *Villin^{Cre}-A$_{2B}$AR$^{fl/fl}$* mice 24 h after inoculation. As shown in Figure 4H, *Il33* mRNA was significantly increased in *Hpb*-inoculated

Villin^{Cre} but not *Villin^{Cre}-A$_{2B}$AR$^{fl/fl}$* mice. Endogenous IL-33 protein is expressed in the intestinal epithelium (Pichery et al., 2012; Liew et al., 2016; Martin and Martin, 2016; Moussion et al., 2008) and can be processed and cleaved to more bioactive forms during inflammation (Lefrancais et al., 2012, 2014). Western blot analysis for IL-33 was performed on whole duodenal intestinal tissue lysates of *Villin^{Cre}* and *Villin^{Cre}-A$_{2B}$AR$^{fl/fl}$* mice 24 h after inoculation. As shown in Figure 5A, blotting with IL-33 Ab (polyclonal goat-immunoglobulin G [IgG]-Ser109-Ile266) western blot revealed full-length pro-IL-33 in naive and inoculated

**Figure 5. A$_{2B}$AR signaling on IECs activates and induces the production of IL-33 and type 2 markers**

(A–D) *Villin^{Cre}-A$_{2B}$AR$^{fl/fl}$* and corresponding control *Villin^{Cre}* mice were orally inoculated with 200 *Hpb* L3 for 24 h; controls included naive mice orally gavaged with PBS. Western blot analysis of IL-33 was performed on whole duodenal intestinal tissue lysates from naive and *Hpb*-inoculated mice (A). Immunofluorescence staining for IL-33 was detected with anti-IL-33 (green), epithelial cells with anti-EpCAM (red), and nuclear stain Hoechst 3342 (blue) in the proximal small intestine at 20× and 60× (B and C). Quantitation of IL-33$^+$ cells (D).

(E–I) *Villin^{Cre}-A$_{2B}$AR$^{fl/fl}$* and corresponding control *Villin^{Cre}* mice were orally inoculated with 200 *Hpb* L3 for 48 h; controls included naive mice orally gavaged with PBS. RNA from sorted lamina propria (LP) cells (EpCAM$^-$CD45$^+$DAPI$^-$) was extracted and analyzed by qPCR for type 2 cytokines and M2 macrophage markers. Blot was cropped to center on an area of interest. Scale bar, 100 μm for 20× and 25 μm for 60× magnification.

Data shown are the means and SEMs from 3 individual mice per group and are representative of at least 2 independent experiments (1-way ANOVA, multiple comparisons; *p < 0.05, **p < 0.01, ***p < 0.001).

duodenal tissue in both untreated *Villin^{Cre}* and *Villin^{Cre}-A$_{2B}$AR$^{fl/fl}$* mice. In contrast, after infection, the mature (m)IL-33 cleaved bioactive products of IL-33 (~21.18 10 kDa) were observed in *Hpb*-inoculated *Villin^{Cre}* mice, but corresponding bands were less intense in inoculated *Villin^{Cre}-A$_{2B}$AR$^{fl/fl}$* mice. Quantitation of IL-33 forms relative to total protein control showed significant decreases in bioactive cleaved IL-33 in Hpb-inoculated *Villin^{Cre}-A$_{2B}$AR$^{fl/fl}$* mice (Figures S5A–S5E). To examine IL-33 *in situ*, IL-33 expression in proximal intestinal tissue was detected by immunofluorescent staining of IL-33 (green) and EpCAM (red).

IL-33 was localized throughout the lamina propria (LP) and was significantly increased in *Hpb*-inoculated *Villin^{Cre}* compared to *Hpb*-inoculated *Villin^{Cre}-A$_{2B}$AR$^{fl/fl}$* mice (Figures 5B–5D). In both naive strains, IL-33 was expressed at low levels (Figures S5F and S5G). To determine whether the activation of A$_{2B}$AR on IECs is sufficient to trigger increased IL-33, intestinal enteroids were generated from the proximal intestines of *Villin^{Cre}* and *Villin^{Cre}-A$_{2B}$AR$^{fl/fl}$* mice and stimulated with the A$_{2B}$AR agonist BAY60-6583 (Figure S5H). At 48 h, enteroids were lysed, and IL-33 protein was assessed by western blot analysis. In a
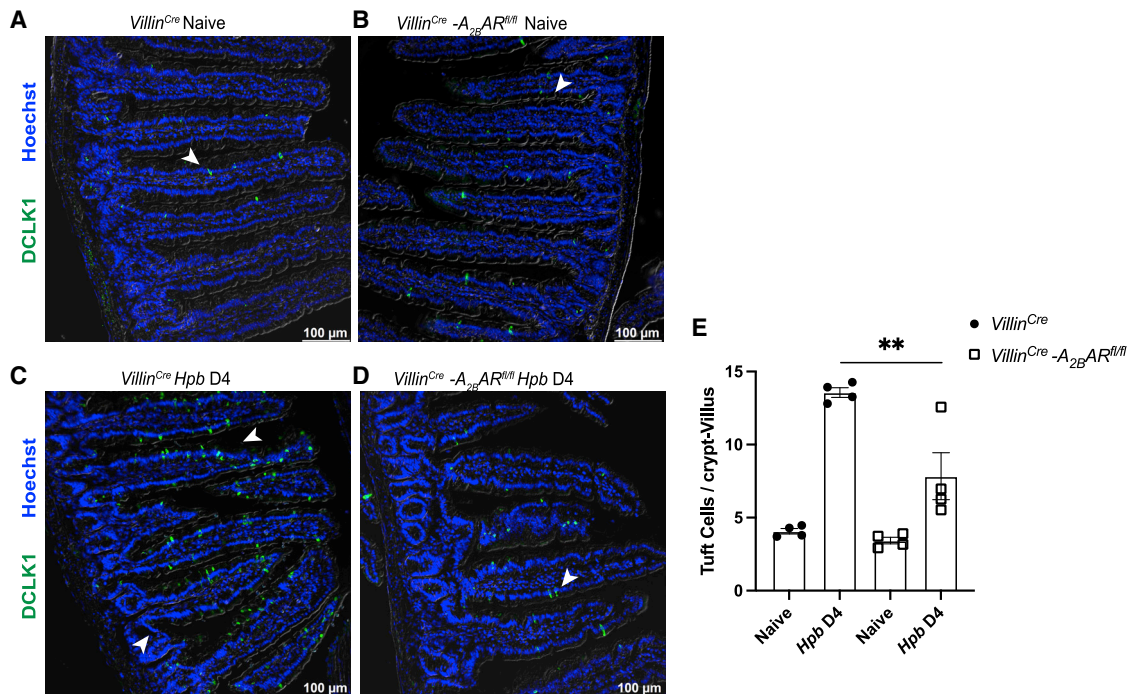
Figure 6. IEC $A_{2B}AR$ signaling contributes to tuft cell hyperplasia
$Villin^{Cre}$-$A_{2B}AR^{fl/fl}$ and control $Villin^{Cre}$ mice were orally inoculated with 200 *Hpb* L3 for 24 h; controls included naive mice orally gavaged with PBS.
(A–D) Tuft cell frequency in the proximal small intestine was assessed by staining with α-DCLK1 (green), marking tuft cells and nuclear stain Hoechst 3342 (blue).
(E) Quantitation of the tuft cells.
Scale bars, 100 μm. Data show the means and SEMs from 4–5 individual mice per group and are representative of at least 2 independent experiments (1-way ANOVA, multiple comparisons; **$p < 0.01$).

separate experiment, enteroids were collected at 24 h to determine *Il33* and $A_{2B}AR$ gene expression. Although $A_{2B}AR$ mRNA was significantly increased in enteroids from $Villin^{Cre}$ mice treated with the agonist, no significant changes in IL-33 protein and mRNA were observed (Figures S5I–S5J). These findings suggest that other factors present *in situ*, such as cytokines and other cell types, contribute to increased bioactive IL-33. We next examined the initial leukocyte type 2 response within the LP. $Villin^{Cre}$ and $Villin^{Cre}$-$A_{2B}AR^{fl/fl}$ mice were infected with *Hpb* for 48 h. LP cells were isolated and sorted ($DAPI^-$ $EpCAM^-$ $CD45^+$) and subjected to qPCR to measure type 2 response genes, including cytokines and M2 markers. Increases in LP $CD45^+$ cells in $Villin^{Cre}$ mice were largely inhibited in $Villin^{Cre}$-$A_{2B}AR^{fl/fl}$ mice, suggesting that $A_{2B}AR$ signaling is required for the initial triggering of the type 2 immune response (Figures 5E–5I), likely due to the decreases in IL-33 specifically in the LP.

Our RNA-seq analysis also revealed a reduction in increases in epithelial cell *Alox5* in $Villin^{Cre}$-$A_{2B}AR^{fl/fl}$ mice after *Hpb* inoculation (Figure 4G). *Alox5* encodes arachidonate 5-lipoxygenase, which plays an essential role in the biosynthesis of leukotrienes that promote the ILC2-tuft cell circuit (Mcginty et al., 2020). The ILC2-tuft cell circuit has been shown to be independent of IL-33 as tuft cell hyperplasia is not significantly reduced in ST2-deficient mice after *Hpb* inoculation (Mcginty et al., 2020). To examine whether tuft cell hyperplasia was also affected by

IEC $A_{2B}AR$ deficiency, $Villin^{Cre}$ and $Villin^{Cre}$-$A_{2B}AR^{fl/fl}$ mice were inoculated with *Hpb*, and 4 days later, proximal intestinal tissues were fixed, frozen in optimal cutting temperature compound (OCT), cryosectioned, and specifically stained with the tuft cell-specific α-DCLK1 monoclonal antibody (mAb) (Mcginty et al., 2020). As shown in Figure 6, pronounced increases in tuft cell hyperplasia observed in $Villin^{Cre}$ mice were inhibited in $Villin^{Cre}$-$A_{2B}AR^{fl/fl}$ mice. These studies indicate that IEC $A_{2B}AR$ deficiency results in pronounced decreases in epithelial cell activation, resulting in impaired IL-33 production and also tuft cell hyperplasia.

Adenosine metabolized from eATP promotes type 2 immune response through triggering epithelial $A_{2B}AR$ signaling

Our findings indicated that shortly after *Hpb* infection, IEC $A_{2B}AR$ blockade compromised IEC activation. To examine the source of adenosine at this early stage of the response, we hypothesized that eATP may play a critical role. To determine the timing of ATP release after *Hpb* inoculation, we used a transgenic ATP reporter mouse that constitutively and ubiquitously expresses a chimeric luciferase (pmeLUC) on the surface of all of the cells. This topology enables pmeLUC to measure ATP increases in the close vicinity of the plasma membrane as luciferase emits light in the presence of ATP and its substrate, luciferin (Di Virgilio et al., 2016). Mice were inoculated with PBS or 200 L3 and
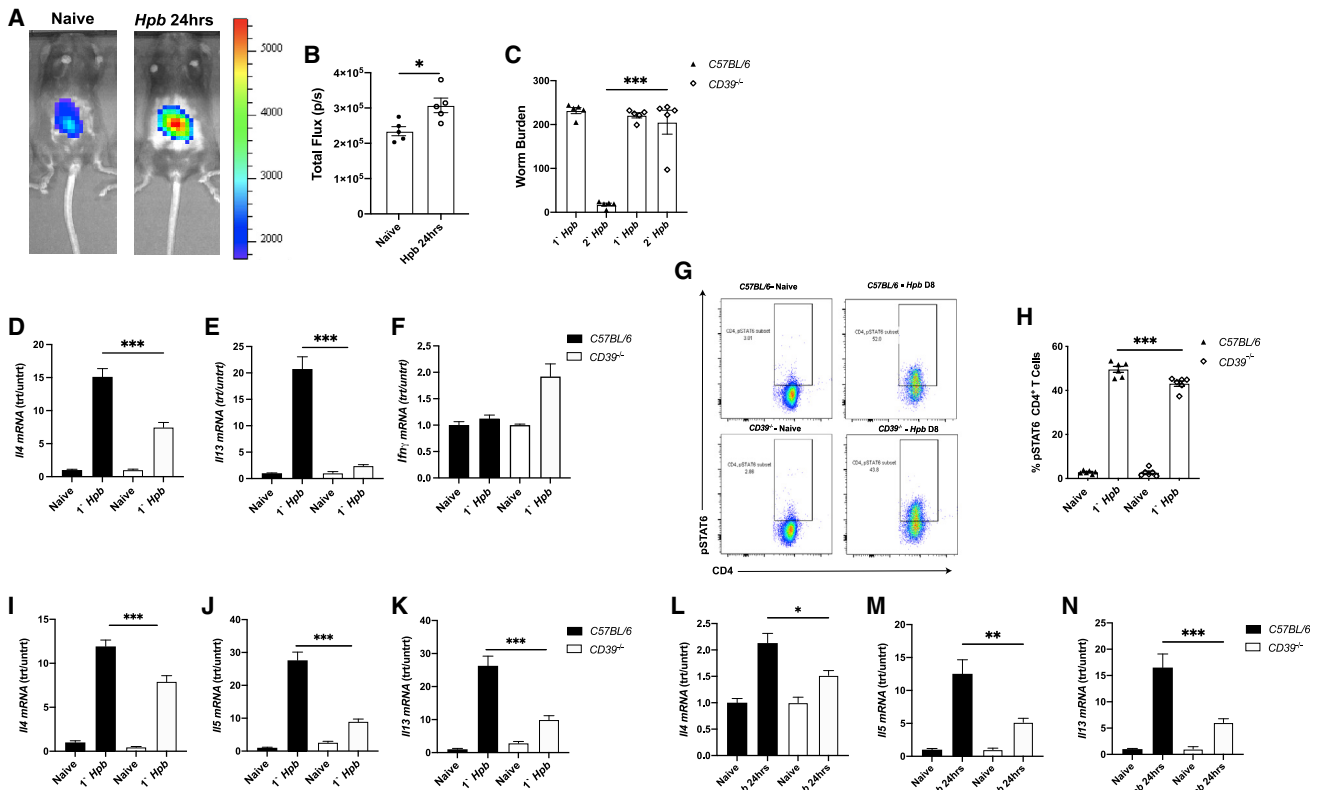
Figure 7. Adenosine metabolized from extracellular ATP promotes type 2 immunity through triggering A$_{2B}$AR signaling on IECs

(A and B) *pmeLuc* mice were orally inoculated with 200 L3 *Hpb* or PBS vehicle. Mice were imaged 24 h post-gavage using the Xenogen IVIS-200 System for the detection of ATP (A) and measurement of total flux (B).

(C) *CD39$^{-/-}$* mice and *WT* controls were orally inoculated with 200 L3 *Hpb*. Mice were treated with pyrantel pamoate 14 days later. At 6 weeks post-clearance, mice were challenged with a 2′ *Hpb* inoculation; controls included naive mice given 1′ *Hpb* inoculation. Resistance was assessed on day 14 by determining luminal worm burden. *CD39$^{-/-}$* mice and WT controls were infected with 200 L3 *Hpb* for 8 days, and controls included naive mice orally gavaged with PBS.

(D–F) MLN tissue was analyzed by qPCR for type 2 and type 1 cytokines.

(G and H) Cell suspensions from MLNs were assessed for intracellular pSTAT6 cell surface expression by CD4$^+$ T cells, with a representative plot (G) and mean percentage of CD4$^+$ T cells expressing pSTAT6 (H). (I–N) Small intestinal tissue was analyzed by qPCR for type 2 cytokines at 8 days (I–K) and 24 h after inoculation (I–N). Data from both experiments show the means and SEMs from 4–5 individual mice per group and are representative of at least 2 independent experiments (1-way ANOVA, multiple comparisons; *p < 0.05, **p < 0.01, ***p < 0.001).

imaged 24 h post-inoculation. Ten minutes before imaging, mice were injected intraperitoneally with D-luciferin (75 mg/kg). Our studies demonstrate ATP release within 24 h post-*Hpb* inoculation (Figures 7A and 7B). eATP can be degraded into extracellular adenosine by cell surface ectonucleotidases CD39 and CD73 (Zimmermann, 2000; Linden, 2001; Thompson et al., 2004; Antonioli et al., 2013a, 2013b, 2015). We have previously reported that intestinal epithelial lymphocytes (IELs) increase the surface expression of CD39 and CD73 within 24 h of *Hpb* inoculation (Patel et al., 2014). To examine whether CD39 and, by extension, adenosine derived from eATP, contributed to the host protective memory response to *Hpb*, *CD39$^{-/-}$* and *WT* controls were inoculated orally with 200 L3 *Hpb* (1′*Hpb*), and 14 days later, mice were drug treated to remove parasites from the gut (Anthony et al., 2006). At 6 weeks post-clearance, *CD39$^{-/-}$* and *WT* control mice were challenged with a secondary inoculation of 200 L3 *Hpb* (2′*Hpb*), and control groups of naive *CD39$^{-/-}$* and *WT* mice were given a primary (1′) *Hpb* inoculation. Fourteen

days later, *WT* mice had a reduced worm burden consistent with an effective type 2 memory response, while *CD39$^{-/-}$* mice had significant and pronounced increases in worm burden, comparable to worm burdens associated with the primary response (Figure 7C). As such, the type 2 memory-protective response was essentially abrogated. To assess the primary response, *CD39$^{-/-}$* *WT* control mice were infected with *Hpb* for 8 days. Mice lacking CD39 showed impaired type 2 cytokine expression in the MLNs (Figures 7D–7F). The MLN CD4$^+$, pSTAT6$^+$ T cell population, which was used as an indicator of IL-4/IL-13 bioactivity (Perona-Wright et al., 2010; Patel et al., 2014), was significantly decreased in *CD39$^{-/-}$* mice when compared to *WT* mice (Figures 7G and 7H). Furthermore, type 2 cytokines in small intestinal tissue from *CD39$^{-/-}$* mice also showed a significant decrease compared to *WT* controls (Figures 7I–7K). However, although decreased, there was still significant type 2 cytokine bioactivity at this later stage of the primary response. To examine whether CD39 played a role in the initiation of the response,

$CD39^{-/-}$ mice and *WT* controls were inoculated with *Hpb*, and 24 h later, the small intestine was collected, and RNA was isolated for qPCR analyses. *Hpb*-inoculated $CD39^{-/-}$ mice had significantly impaired expression of type 2 cytokines (Figures 7I–7N). These results indicate that eATP is metabolized to adenosine, which then acts as an essential endogenous danger signal for the initiation of type 2 immune response and development of the subsequent memory response.

DISCUSSION

Our results indicate a significant role for adenosine, specifically binding $A_{2B}AR$ on IECs in driving a host protective memory immune response to the nematode parasite, *Hpb*. We further show that $A_{2B}AR$ signaling is required for the development of memory $CD4^+$ T cells but not for their subsequent activation during the memory response. During the primary response, $A_{2B}AR$ signaling in IECs markedly promotes the initial activation of innate immunity through multiple mechanisms. The source of adenosine is eATP, which is released locally after infection, with the ectonucleotidase CD39 playing an essential role in the generation of adenosine.

The increased eATP observed by 24 h after *Hpb* inoculation is likely a result of tissue damage caused by parasites crossing the epithelial barrier. Previous studies have shown that eATP binds P2X7 receptor eATP on mast cells, triggering their production of IL-33 and promoting host protection in $Spi-B^{-/-}$ mice with constitutively increased mast cells (Shimokawa et al., 2017). Our studies show that eATP catabolized to adenosine plays an essential role in driving the initial innate type 2 immune response during helminth infection. Our findings indicate that IEC $A_{2B}AR$ signaling is essential for both cleavage of IL-33 to more active forms and increased IEC *Il33* mRNA, the latter likely promoting sustained IL-33 production. Previous studies showing that the administration of IL-33 in global $A_{2B}AR^{-/-}$ mice restores early innate type 2 immunity is consistent with IL-33 playing an intermediary role in the initiation of type 2 immunity by adenosine signaling (Patel et al., 2014). Tuft cells have also been shown to be important in driving the type 2 response to helminths (Gerbe et al., 2016; Mcginty et al., 2020; Nadjsombati et al., 2018; Von Moltke and Pepper, 2018; Von Moltke et al., 2016), and this specialized epithelial cell can respond to helminth infection by the production of cysteine leukotrienes, which, together with constitutive IL-25 promotes tuft cell hyperplasia (Smith et al., 2018). Our findings that *Alox5*, which mediates the production of cysteine leukotrienes (Mcginty et al., 2020), was reduced in *Hpb*-inoculated $Villin^{Cre}-A_{2B}AR^{fl/fl}$ mice and that tuft cell hyperplasia, contributing to anti-helminth responses, was markedly inhibited indicates a critical role for IEC $A_{2B}AR$ signaling in this important pathway promoting type 2 immunity. Tuft cell hyperplasia is IL-33 independent (Von Moltke et al., 2016), suggesting a more direct effect of $A_{2B}AR$ signaling on tuft cells. Indeed, previous studies have indicated a role for $A_{2B}AR$ signaling in taste bud sensing of sweet taste (Dando et al., 2012; Kataoka et al., 2012).

$A_{2B}AR$ signaling at the intestinal mucosal surface is also associated with inflammatory bowel diseases (IBDs) such as Crohn's disease and ulcerative colitis (Frick et al., 2009; Aherne et al.,

2015; Kolachala et al., 2005). It can contribute to intestinal fluid secretion, colonic motility, and immune activation (Antonioli et al., 2008; Kolachala et al., 2006). The upregulation of $A_{2B}AR$ in the intestinal epithelium has been shown to induce chloride secretion through a cyclic AMP (cAMP)-dependent pathway (Strohmeier et al., 1995), as well as increases in intracellular cAMP leading to activation of protein kinase A (PKA) (Kolachala et al., 2006), and the deletion of the $A_{2B}AR$ receptor leads to decreases in IL-10 expression, exacerbating colitis (Frick et al., 2009). The $A_{2B}AR$ receptor can also activate PLC via $G\alpha_q$ signaling, inducing Ca^+ mobilization (Linden et al., 1998). As $A_{2B}AR$ signaling did not directly induce increased IL-33 production or bioactive cleavage products in the intestinal enteroids treated with the $A_{2B}AR$ agonist, other *in vivo* signals are likely needed. For example, proteases from mast cells and neutrophil serine proteases, cathepsin G, and elastase can cleave extracellular IL-33 (Lefrancais et al., 2012, 2014). Of note, the RNA-seq analysis of IECs after *Hpb* infection showed that $A_{2B}AR$ signaling on epithelial cells triggered $G\alpha_s$ and $G\alpha_q$ proteins and PLC signaling consistent with these pathways mediating $A_{2B}AR$ induction of the IEC response to *Hpb*. PLC has also been shown to induce Ca^+ mobilization and mast cell degranulation, leading to IL-33 cleavage into bioactive forms (Lefrancais et al., 2012, 2014).

We now demonstrate that IEC, but not myeloid cell, $A_{2B}AR$ signaling drives the early primary and the memory response to this enteric helminth. Epithelial cells are likely of particular importance at barrier surfaces in triggering type 2 responses, allowing them to serve as sentinel cells capable of rapidly inducing innate immunity following the sensing of helminth-associated signals or as a result of direct cellular stress or damage. In contrast, in the peritoneum, the deletion of $A_{2B}AR$ in myeloid cells blocked the type 2 immune responses to sterile MPs. This is consistent with previous studies showing an essential role for macrophages in producing IL-33 in this type 2 sterile inflammation model (Mishra et al., 2019). Our findings now demonstrate the general significance of $A_{2B}AR$ signaling in driving type 2 immunity even though the tissue microenvironment and essential type 2 response-inducing cell types are distinct.

Our analysis of the characteristic type 2 granuloma at the host-parasite interface following secondary inoculation showed profound decreases in M2 macrophages in IEC $A_{2B}AR$-deficient mice. Previous studies have shown that M2 macrophages impair larval parasite development during the tissue-dwelling phase (Anthony et al., 2006; Esser-von Bieren et al., 2013). As the parasite life cycle includes only a short 8-day tissue-dwelling window, when macrophages and other cell types can directly interact with and damage the developing larvae, the rapid activation of memory T cells that drive granuloma development is likely critical for accelerated resistance after secondary inoculation. Our adoptive transfer experiments revealed that IEC $A_{2B}AR$ signaling is not required for the activation of memory T cells after secondary exposure. Consistent with these findings, we further showed in analogous transfer experiments that the activation of memory T cells was also refractory to a requirement for IL-4 in recipient naive mice. Previous studies have shown that memory T cell activation following a secondary challenge is less dependent on certain extrinsic signals, such

as co-stimulatory molecules, than the actual formation of memory T cells during the primary response (Minutti et al., 2017; Chang et al., 2014; Gause et al., 1997). Indeed, our findings showed that $A_{2B}AR$ epithelial cell signaling is preferentially required for the development of memory Th2 cells rather than their subsequent activation.

Our observation, using *pmeLuc* reporter mice, that eATP is markedly increased at 24 h after *Hpb* inoculation, raised the possibility that the eATP may be an important source of adenosine. However, it was also possible that intracellular adenosine secreted through the nucleoside transporter (Young, 2016; Boswell-Casteel and Hays, 2017) could be the primary source. eATP is metabolized to adenosine through cell surface CD39 and CD73. We had previously shown that CD39 and CD73 were upregulated in intestinal epithelial lymphocytes but not in LP lymphocytes shortly after *Hpb* inoculation, which generally correlates with the increased release and degradation of eATP into adenosine (Patel et al., 2014; Antonioli et al., 2013b). Our findings in $CD39^{-/-}$ mice now demonstrate that eATP is a critical source of the adenosine essential in driving the *Hpb*-induced type 2 immune response. It should be noted that while ATP is the most likely nucleotide degraded by CD39 in our system, it is also possible that CD39-mediated degradation of other nucleotides, such as adenosine diphosphate (ADP), uridine-5′-triphosphate (UTP), and uridine-5′-diphosphate (UDP), may play a role in driving type 2 immunity. Additional studies will be required to study in detail the role of these nucleotides. It should also be noted that CD73 and not CD39 is expressed on IECs (Kao et al., 2017). It is clear from the literature that CD39 and CD73 do not need to be co-expressed by the same cell to generate adenosine. In fact, in many tissues, CD39 expressed by one cell will provide AMP to CD73 expressed on another cell, resulting in the efficient generation of adenosine in the tissue (Antonioli et al., 2013b). Since many immune cell types, including macrophages, neutrophils, and lymphocytes, can express CD39, it is likely that collaboration between CD73 on IECs and CD39 on immune cells is responsible for adenosine production.

Although the IEC response and the early cytokine response were largely blocked by IEC $A_{2B}AR$ blockade following primary *Hpb* inoculation, at later stages, the type 2 response was partially restored, indicating that other factors may become stimulated as the response progresses that can at least to some extent substitute for the adenosine-dependent IEC response, similar to the partial suppression observed at later stages of the helminth response when the ILC2-tuft cell circuit is inhibited (Mcginty et al., 2020; Schneider et al., 2018). Interestingly, effector T cell activation is also refractory to IL-33 blockade during helminth infection (Hung et al., 2013). In contrast, our findings that the CD4-dependent memory response leading to accelerated worm expulsion was largely abrogated following IEC $A_{2B}AR$ blockade suggests an obligatory role for this initial IEC activation in memory T cell development during the primary response. At later stages of the primary response, memory effector cells may not develop as readily, particularly as the parasites exit the intestinal tissues and return to the lumen by day 8 after infection. This initial tissue-dwelling phase may be associated with a potent stimulation of the immune response that favors memory

T cell differentiation. Future studies are needed to elucidate the specific factors that contribute to memory T cell development at these initial stages of type 2 immunity.

In summary, our studies indicate that adenosine, derived from eATP, triggers IEC $A_{2B}AR$ signaling, resulting in differential activation of epithelial cells following intestinal helminth infection. This activation is required for the initiation of type 2 innate immunity, and its absence impairs the development of memory Th2 cells, essential for acquired resistance. Taken together, these results suggest that multiple successive signals progressively fine-tune the upregulation of the type 2 immune response. This may play an important role in controlling the potency of type 2 immune responses, potentially minimizing associated harmful effects.

Limitations of the study

A limitation of this study is that our findings do not directly address how the formation of memory CD4^{+} T cells is inhibited during the primary response in mice deficient in the $A_{2B}AR$ receptor on IECs. Although we suspect it is related to the impaired innate immunity observed at the early stages of the primary response, identification of antigen-specific T cells, not available in this enteric murine *Hpb* parasite model, would greatly facilitate such studies. Furthermore, although we identified the eATP-CD39 axis as the pathway of eATP degradation into adenosine within 24 h of infection, other nucleotides could also be involved, including ADP, UTP, and UDP, in driving type 2 immunity. It should also be noted that helminth infections may facilitate commensal bacteria crossing the intestinal barrier, potentially contributing to the overall response.

STAR★METHODS

Detailed methods are provided in the online version of this paper and include the following:

Cell Reports
Article

AUTHOR CONTRIBUTIONS

Conceptualization, W.C.G., G.H., D.W.E., F.C., and K.L.E.; methodology, W.C.G., G.H., D.W.E., and F.C.; formal analysis, D.W.E., W.C.G., and A.L.; investigation, D.W.E., F.C., M.J.P., P.K.M., M.A.F., and W.W.; resources, H.K.E., F.D.V., S.C.R., and G.S.Y.; data curation, W.C.G. and D.W.E.; writing – original draft, D.W.E. and W.C.G.; and writing – review & editing, D.W.E., W.C.G., and G.H.

REFERENCES

Aherne, C.M., Saeedi, B., Collins, C.B., Masterson, J.C., Mcnamee, E.N., Perrenoud, L., Rapp, C.R., Curtis, V.F., Bayless, A., Fletcher, A., et al. (2015). Epithelial-specific A2B adenosine receptor signaling protects the colonic epithelial barrier during acute colitis. Mucosal Immunol. 8, 1324–1338.

Anthony, R.M., Rutitzky, L.I., Urban, J.F., Jr., Stadecker, M.J., and Gause, W.C. (2007). Protective immune mechanisms in helminth infection. Nat. Rev. Immunol. 7, 975–987.

Anthony, R.M., Urban, J.F., Jr., Alem, F., Hamed, H.A., Rozo, C.T., Boucher, J.L., Van Rooijen, N., and Gause, W.C. (2006). Memory T(H)2 cells induce alternatively activated macrophages to mediate protection against nematode parasites. Nat. Med. 12, 955–960.

Antonioli, L., Fornai, M., Colucci, R., Ghisu, N., Tuccori, M., Del Tacca, M., and Blandizzi, C. (2008). Regulation of enteric functions by adenosine: pathophysiological and pharmacological implications. Pharmacol. Ther. 120, 233–253.

Antonioli, L., Blandizzi, C., Pacher, P., and Haskó, G. (2013a). Immunity, inflammation and cancer: a leading role for adenosine. Nat. Rev. Cancer 13, 842–857.

Antonioli, L., Pacher, P., Vizi, E.S., and Haskó, G. (2013b). CD39 and CD73 in immunity and inflammation. Trends Mol. Med. 19, 355–367.

Antonioli, L., Blandizzi, C., Csóka, B., Pacher, P., and Haskó, G. (2015). Adenosine signalling in diabetes mellitus–pathophysiology and therapeutic considerations. Nat. Rev. Endocrinol. 11, 228–241.

Boswell-Casteel, R.C., and Hays, F.A. (2017). Equilibrative nucleoside transporters-A review. Nucleos Nucleot. Nucleic Acids 36, 7–30.

Chang, J.T., Wherry, E.J., and Goldrath, A.W. (2014). Molecular regulation of effector and memory T cell differentiation. Nat. Immunol. 15, 1104–1115.

Clausen, B.E., Burkhardt, C., Reith, W., Renkawitz, R., and Förster, I. (1999). Conditional gene targeting in macrophages and granulocytes using LysMcre mice. Transgenic Res. 8, 265–277.

Csoka, B., Koscsó, B., Töro, G., Kókai, E., Virág, L., Németh, Z.H., Pacher, P., Bai, P., and Haskó, G. (2014). A2B adenosine receptors prevent insulin resistance by inhibiting adipose tissue inflammation via maintaining alternative macrophage activation. Diabetes 63, 850–866.

Csoka, B., Németh, Z.H., Duerr, C.U., Fritz, J.H., Pacher, P., and Haskó, G. (2018a). Adenosine receptors differentially regulate type 2 cytokine production by IL-33-activated bone marrow cells, ILC2s, and macrophages. FASEB J. 32, 829–837.

Csoka, B., Németh, Z.H., Szabó, I., Davies, D.L., Varga, Z.V., Pálóczi, J., Falzoni, S., Di Virgilio, F., Muramatsu, R., Yamashita, T., et al. (2018b). Macrophage P2X4 receptors augment bacterial killing and protect against sepsis. JCI Insight 3, 99431.

Csoka, B., Selmeczy, Z., Koscsó, B., Németh, Z.H., Pacher, P., Murray, P.J., Kepka-Lenhart, D., Morris, S.M., Jr., Gause, W.C., Leibovich, S.J., and Haskó, G. (2012). Adenosine promotes alternative macrophage activation via A2A and A2B receptors. Faseb. J. 26, 376–386.

Dando, R., Dvoryanchikov, G., Pereira, E., Chaudhari, N., and Roper, S.D. (2012). Adenosine enhances sweet taste through A2B receptors in the taste bud. J. Neurosci. 32, 322–330.

Di Virgilio, F., Pinton, P., and Falzoni, S. (2016). Assessing extracellular ATP as danger signal in vivo: the pmeLuc system. Methods Mol. Biol. 1417, 115–129.

El-Naccache, D.W., Hasko, G., and Gause, W.C. (2020). Early events triggering the initiation of a type 2 immune response. Trends Immunol. 42, 151–164.

Enjyoji, K., Sévigny, J., Lin, Y., Frenette, P.S., Christie, P.D., Esch, J.S., 2nd, Imai, M., Edelberg, J.M., Rayburn, H., Lech, M., et al. (1999). Targeted disruption of cd39/ATP diphosphohydrolase results in disordered hemostasis and thromboregulation. Nat. Med. 5, 1010–1017.

Esser-Von Bieren, J., Mosconi, I., Guiet, R., Piersgilli, A., Volpe, B., Chen, F., Gause, W.C., Seitz, A., Verbeek, J.S., and Harris, N.L. (2013). Antibodies trap tissue migrating helminth larvae and prevent tissue damage by driving IL-4Ralpha-independent alternative differentiation of macrophages. PLoS Pathog. 9, e1003771.

Faniyi, A.A., Wijanarko, K.J., Tollitt, J., and Worthington, J.J. (2020). Helminth sensing at the intestinal epithelial barrier-A taste of things to come. Front. Immunol. 11, 1489.

Finkelman, F.D., Shea-Donohue, T., Goldhill, J., Sullivan, C.A., Morris, S.C., Madden, K.B., Gause, W.C., and Urban, J.F., Jr. (1997). Cytokine regulation of host defense against parasitic gastrointestinal nematodes: lessons from studies with rodent models. Annu. Rev. Immunol. 15, 505–533.

Frick, J.S., Macmanus, C.F., Scully, M., Glover, L.E., Eltzschig, H.K., and Colgan, S.P. (2009). Contribution of adenosine A2B receptors to inflammatory parameters of experimental colitis. J. Immunol. 182, 4957–4964.

Gause, W.C., Mitro, V., Via, C., Linsley, P., Urban, J.F., Jr., and Greenwald, R.J. (1997). Do effector and memory T helper cells also need B7 ligand costimulatory signals? J. Immunol. 159, 1055–1058.

Gause, W.C., Rothlin, C., and Loke, P. (2020). Heterogeneity in the initiation, development and function of type 2 immunity. Nat. Rev. Immunol. 20, 603–614.

Gerbe, F., Sidot, E., Smyth, D.J., Ohmoto, M., Matsumoto, I., Dardalhon, V., Cesses, P., Garnier, L., Pouzolles, M., Brulin, B., et al. (2016). Intestinal epithelial tuft cells initiate type 2 mucosal immunity to helminth parasites. Nature 529, 226–230.

Haber, A.L., Biton, M., Rogel, N., Herbst, R.H., Shekhar, K., Smillie, C., Burgin, G., Delorey, T.M., Howitt, M.R., Katz, Y., et al. (2017). A single-cell survey of the small intestinal epithelium. Nature 551, 333–339.

Hart, M.L., Jacobi, B., Schittenhelm, J., Henn, M., and Eltzschig, H.K. (2009). Cutting Edge: a2B Adenosine receptor signaling provides potent protection during intestinal ischemia/reperfusion injury. J. Immunol. 182, 3965–3968.

Heine, P., Braun, N., Sévigny, J., Robson, S.C., Servos, J., and Zimmermann, H. (2001). The C-terminal cysteine-rich region dictates specific catalytic

properties in chimeras of the ectonucleotidases NTPDase1 and NTPDase2. Eur. J. Biochem. *268*, 364–373.

Herbert, D.R., Yang, J.Q., Hogan, S.P., Groschwitz, K., Khodoun, M., Munitz, A., Orekov, T., Perkins, C., Wang, Q., Brombacher, F., et al. (2009). Intestinal epithelial cell secretion of RELM-beta protects against gastrointestinal worm infection. J. Exp. Med. *206*, 2947–2957.

Humphreys, N.E., Xu, D., Hepworth, M.R., Liew, F.Y., and Grencis, R.K. (2008). IL-33, a potent inducer of adaptive immunity to intestinal nematodes. J. Immunol. *180*, 2443–2449.

Hung, L.Y., Lewkowich, I.P., Dawson, L.A., Downey, J., Yang, Y., Smith, D.E., and Herbert, D.R. (2013). IL-33 drives biphasic IL-13 production for noncanonical Type 2 immunity against hookworms. Proc. Natl. Acad. Sci. USA *110*, 282–287.

Kao, D.J., Saeedi, B.J., Kitzenberg, D., Burney, K.M., Dobrinskikh, E., Battista, K.D., Vázquez-Torres, A., Colgan, S.P., and Kominsky, D.J. (2017). Intestinal epithelial ecto-5′-nucleotidase (CD73) regulates intestinal colonization and infection by nontyphoidal Salmonella. Infect. Immun. *85*, e01022-16.

Kataoka, S., Baquero, A., Yang, D., Shultz, N., Vandenbeuch, A., Ravid, K., Kinnamon, S.C., and Finger, T.E. (2012). A2BR adenosine receptor modulates sweet taste in circumvallate taste buds. PLoS One *7*, e30032.

Knapp, K., Zebisch, M., Pippel, J., El-Tayeb, A., Müller, C.E., and Sträter, N. (2012). Crystal structure of the human ecto-5′-nucleotidase (CD73): insights into the regulation of purinergic signaling. Structure *20*, 2161–2173.

Kolachala, V.L., Obertone, T.S., Wang, L., Merlin, D., and Sitaraman, S.V. (2006). Adenosine 2b receptor (A2bR) signals through adenylate cyclase (AC) 6 isoform in the intestinal epithelial cells. Biochim. Biophys. Acta *1760*, 1102–1108.

Kolachala, V., Asamoah, V., Wang, L., Obertone, T.S., Ziegler, T.R., Merlin, D., and Sitaraman, S.V. (2005). TNF-alpha upregulates adenosine 2b (A2b) receptor expression and signaling in intestinal epithelial cells: a basis for A2bR overexpression in colitis. Cell. Mol. Life Sci. *62*, 2647–2657.

Koscso, B., Csóka, B., Kókai, E., Németh, Z.H., Pacher, P., Virág, L., Leibovich, S.J., and Haskó, G. (2013). Adenosine augments IL-10-induced STAT3 signaling in M2c macrophages. J. Leukoc. Biol. *94*, 1309–1315.

Lefrancais, E., Duval, A., Mirey, E., Roga, S., Espinosa, E., Cayrol, C., and Girard, J.P. (2014). Central domain of IL-33 is cleaved by mast cell proteases for potent activation of group-2 innate lymphoid cells. Proc. Natl. Acad. Sci. USA *111*, 15502–15507.

Lefrancais, E., Roga, S., Gautier, V., Gonzalez-De-Peredo, A., Monsarrat, B., Girard, J.P., and Cayrol, C. (2012). IL-33 is processed into mature bioactive forms by neutrophil elastase and cathepsin G. Proc. Natl. Acad. Sci. USA *109*, 1673–1678.

Liew, F.Y., Girard, J.P., and Turnquist, H.R. (2016). Interleukin-33 in health and disease. Nat. Rev. Immunol. *16*, 676–689.

Linden, J. (2001). Molecular approach to adenosine receptors: receptor-mediated mechanisms of tissue protection. Annu. Rev. Pharmacol. Toxicol. *41*, 775–787.

Linden, J., Auchampach, J.A., Jin, X., and Figler, R.A. (1998). The structure and function of A1 and A2B adenosine receptors. Life Sci. *62*, 1519–1524.

Madison, B.B., Dunbar, L., Qiao, X.T., Braunstein, K., Braunstein, E., and Gumucio, D.L. (2002). Cis elements of the villin gene control expression in restricted domains of the vertical (crypt) and horizontal (duodenum, cecum) axes of the intestine. J. Biol. Chem. *277*, 33275–33283.

Martin, N.T., and Martin, M.U. (2016). Interleukin 33 is a guardian of barriers and a local alarmin. Nat. Immunol. *17*, 122–131.

Mcginty, J.W., Ting, H.A., Billipp, T.E., Nadjsombati, M.S., Khan, D.M., Barrett, N.A., Liang, H.E., Matsumoto, I., and Von Moltke, J. (2020). Tuft-cell-derived leukotrienes drive rapid anti-helminth immunity in the small intestine but are dispensable for anti-protist immunity. Immunity *52*, 528–541.e7.

Minutti, C.M., Drube, S., Blair, N., Schwartz, C., Mccrae, J.C., Mckenzie, A.N., Kamradt, T., Mokry, M., Coffer, P.J., Sibilia, M., et al. (2017). Epidermal Growth factor receptor expression licenses type-2 helper T cells to function in a T cell receptor-independent fashion. Immunity *47*, 710–722.e6.

Mishra, P.K., Palma, M., Buechel, B., Moore, J., Davra, V., Chu, N., Millman, A., Hallab, N.J., Kanneganti, T.D., Birge, R.B., et al. (2019). Sterile particle-induced inflammation is mediated by macrophages releasing IL-33 through a Bruton's tyrosine kinase-dependent pathway. Nat. Mater. *18*, 289–297.

Mishra, P.K., Wu, W., Rozo, C., Hallab, N.J., Benevenia, J., and Gause, W.C. (2011). Micrometer-sized titanium particles can induce potent Th2-type responses through TLR4-independent pathways. J. Immunol. *187*, 6491–6498.

Morimoto, M., Morimoto, M., Whitmire, J., Xiao, S., Anthony, R.M., Mirakami, H., Star, R.A., Urban, J.F., Jr., and Gause, W.C. (2004). Peripheral CD4 T cells rapidly accumulate at the host: parasite interface during an inflammatory Th2 memory response. J. Immunol. *172*, 2424–2430.

Moussion, C., Ortega, N., and Girard, J.P. (2008). The IL-1-like cytokine IL-33 is constitutively expressed in the nucleus of endothelial cells and epithelial cells in vivo: a novel 'alarmin. PLoS One *3*, e3331.

Nadjsombati, M.S., Mcginty, J.W., Lyons-Cohen, M.R., Jaffe, J.B., Dipeso, L., Schneider, C., Miller, C.N., Pollack, J.L., Nagana Gowda, G.A., Fontana, M.F., et al. (2018). Detection of succinate by intestinal tuft cells triggers a type 2 innate immune circuit. Immunity *49*, 33–41.e7.

Patel, N., Wu, W., Mishra, P.K., Chen, F., Millman, A., Csóka, B., Koscsó, B., Eltzschig, H.K., Haskó, G., and Gause, W.C. (2014). A2B adenosine receptor induces protective antihelminth type 2 immune responses. Cell Host Microbe *15*, 339–350.

Perona-Wright, G., Mohrs, K., and Mohrs, M. (2010). Sustained signaling by canonical helper T cell cytokines throughout the reactive lymph node. Nat. Immunol. *11*, 520–526.

Pichery, M., Mirey, E., Mercier, P., Lefrancais, E., Dujardin, A., Ortega, N., and Girard, J.P. (2012). Endogenous IL-33 is highly expressed in mouse epithelial barrier tissues, lymphoid organs, brain, embryos, and inflamed tissues: in situ analysis using a novel Il-33-LacZ gene trap reporter strain. J. Immunol. *188*, 3488–3495.

Rath, E., Moschetta, A., and Haller, D. (2018). Mitochondrial function - gatekeeper of intestinal epithelial cell homeostasis. Nat. Rev. Gastroenterol. Hepatol. *15*, 497–516.

Reynolds, L.A., Filbey, K.J., and Maizels, R.M. (2012). Immunity to the model intestinal helminth parasite Heligmosomoides polygyrus. Semin. Immunopathol. *34*, 829–846.

Roan, F., Obata-Ninomiya, K., and Ziegler, S.F. (2019). Epithelial cell-derived cytokines: more than just signaling the alarm. J. Clin. Invest. *129*, 1441–1451.

Ryan, N., Anderson, K., Volpedo, G., Varikuti, S., Satoskar, M., Satoskar, S., and Oghumu, S. (2020). The IL-33/ST2 Axis in immune responses against parasitic disease: potential therapeutic applications. Front. Cell. Infect. Microbiol. *10*, 153.

Ryzhov, S., Goldstein, A.E., Matafonov, A., Zeng, D., Biaggioni, I., and Feoktistov, I. (2004). Adenosine-activated mast cells induce IgE synthesis by B lymphocytes: an A2B-mediated process involving Th2 cytokines IL-4 and IL-13 with implications for asthma. J. Immunol. *172*, 7726–7733.

Schneider, C., O'leary, C.E., Von Moltke, J., Liang, H.E., Ang, Q.Y., Turnbaugh, P.J., Radhakrishnan, S., Pellizzon, M., Ma, A., and Locksley, R.M. (2018). A metabolite-triggered tuft cell-ILC2 circuit drives small intestinal remodeling. Cell *174*, 271–284.e14.

Seo, S.W., Koeppen, M., Bonney, S., Gobel, M., Thayer, M., Harter, P.N., Ravid, K., Eltzschig, H.K., Mittelbronn, M., Walker, L., and Eckle, T. (2015). Differential tissue-specific function of Adora2b in cardioprotection. J. Immunol. *195*, 1732–1743.

Shimokawa, C., Kanaya, T., Hachisuka, M., Ishiwata, K., Hisaeda, H., Kurashima, Y., Kiyono, H., Yoshimoto, T., Kaisho, T., and Ohno, H. (2017). Mast cells are crucial for induction of group 2 innate lymphoid cells and clearance of helminth infections. Immunity *46*, 863–874.e4.

Smith, K.A., Löser, S., Varyani, F., Harcus, Y., Mcsorley, H.J., Mckenzie, A.N., and Maizels, R.M. (2018). Concerted IL-25R and IL-4Ralpha signaling drive innate type 2 effector immunity for optimal helminth expulsion. Elife *7*, e38269.

Strater, N. (2006). Ecto-5′-nucleotidase: structure function relationships. Purinergic Signal. *2*, 343–350.

Strohmeier, G.R., Reppert, S.M., Lencer, W.I., and Madara, J.L. (1995). The A2b adenosine receptor mediates cAMP responses to adenosine receptor agonists in human intestinal epithelia. J. Biol. Chem. *270*, 2387–2394.

Svetic, A., Madden, K.B., Zhou, X.D., Lu, P., Katona, I.M., Finkelman, F.D., Urban, J.F., Jr., and Gause, W.C. (1993). A primary intestinal helminthic infection rapidly induces a gut-associated elevation of Th2-associated cytokines and IL-3. J. Immunol. *150*, 3434–3441.

Thompson, L.F., Eltzschig, H.K., Ibla, J.C., Van De Wiele, C.J., Resta, R., Morote-Garcia, J.C., and Colgan, S.P. (2004). Crucial role for ecto-5′-nucleotidase (CD73) in vascular leakage during hypoxia. J. Exp. Med. *200*, 1395–1405.

Urban, J.F., Jr., Katona, I.M., Paul, W.E., and Finkelman, F.D. (1991). Interleukin 4 is important in protective immunity to a gastrointestinal nematode infection in mice. Proc. Natl. Acad. Sci. USA *88*, 5513–5517.

Vannella, K.M., Ramalingam, T.R., Borthwick, L.A., Barron, L., Hart, K.M., Thompson, R.W., Kindrachuk, K.N., Cheever, A.W., White, S., Budelsky, A.L., et al. (2016). Combinatorial targeting of TSLP, IL-25, and IL-33 in type 2 cytokine-driven inflammation and fibrosis. Sci. Transl. Med. *8*, 337ra65.

Von Moltke, J., and Pepper, M. (2018). Sentinels of the type 2 immune response. Trends Immunol. *39*, 99–111.

Von Moltke, J., Ji, M., Liang, H.E., and Locksley, R.M. (2016). Tuft-cell-derived IL-25 regulates an intestinal ILC2-epithelial response circuit. Nature *529*, 221–225.

Xaus, J., Mirabet, M., Lloberas, J., Soler, C., Lluis, C., Franco, R., and Celada, A. (1999). IFN-gamma up-regulates the A2B adenosine receptor expression in macrophages: a mechanism of macrophage deactivation. J. Immunol. *162*, 3607–3614.

Young, J.D. (2016). The SLC28 (CNT) and SLC29 (ENT) nucleoside transporter families: a 30-year collaborative odyssey. Biochem. Soc. Trans. *44*, 869–876.

Yu, S., Tong, K., Zhao, Y., Balasubramanian, I., Yap, G.S., Ferraris, R.P., Bonder, E.M., Verzi, M.P., and Gao, N. (2018). Paneth cell multipotency induced by notch activation following injury. Cell Stem Cell *23*, 46–59.e5.

Zaiss, M.M., Maslowski, K.M., Mosconi, I., Guenat, N., Marsland, B.J., and Harris, N.L. (2013). IL-1beta suppresses innate IL-25 and IL-33 production and maintains helminth chronicity. PLoS Pathog. *9*, e1003531.

Zimmermann, H. (2000). Extracellular metabolism of ATP and other nucleotides. Naunyn-Schmiedeberg's Arch. Pharmacol. *362*, 299–309.

STAR★METHODS

KEY RESOURCES TABLE

REAGENT or RESOURCE	SOURCE	IDENTIFIER
Antibodies		
APC Rat Anti-Mouse CD4	BD Bioscience	Cat#553051; RRID:AB_398528
PE Mouse Anti-Mouse Stat6 (pY641)	BD Bioscience	Cat#558252; RRID:AB_647233
CD4 (L3T4) MicroBeads, mouse	Miltenyi Biotec	Cat#130-117-043
Mouse IL-4 ELISPOT Pair	BD Bioscience	Cat#551878; RRID:AB_2336921
PE Rat Anti-Mouse CD45	BD Bioscience	Cat#553081; RRID:AB_394611
APC Rat Anti-Mouse CD326	BD Bioscience	Cat#563478; RRID:AB_2738234
TruStain FcX^{TM} (anti-mouse CD16/32) Antibody	BioLegend	Cat#101320 RRID: AB_1574975
Mouse IL-33 Antibody	R&D Systems	Cat#AF3626; RRID:AB_884269
Donkey anti-Goat IgG (H + L) Cross-Adsorbed Secondary Antibody, Alexa Fluor 488	Invitrogen	Cat#A-11055; RRID:AB_2534102
Goat Anti-Rabbit IgG H&L (Alexa Fluor® 488)	Abcam	Cat#ab150077; RRID:AB_2630356
Anti-DCAMKL1	Abcam	Cat#ab31704; RRID:AB_873537
Donkey anti-Goat IgG Secondary Antibody [HRP (Horseradish Peroxidase)]	Novus Biologicals	Cat#HAF109; RRID:AB_357236
Alexa Fluor 488 anti-mouse F4/80 Antibody	BioLegend	Cat#123120; RRID:AB_893479
Alexa Fluor 647 anti-mouse CD206 (MMR) Antibody	BioLegend	Cat#141712; RRID:AB_10900420
Alexa Fluor 488 anti-mouse Ly-6G Antibody	BioLegend	Cat#127626; RRID:AB_2561340
Alexa Fluor® 647 anti-mouse CD4 Antibody	Biolegend	Cat#100530; RRID:AB_389325
Alexa Fluor® 488 Rat IgG2a, κ Isotype Ctrl Antibody	Biolegend	Cat#400525; RRID:AB_2864283
Alexa Fluor® 647 Rat IgG2a, κ Isotype Ctrl Antibody	Biolegend	Cat#400526; RRID:AB_2864284
Chemicals, peptides, andrecombinant proteins		
BAY 60–6583 - Potent A_{2B} agonist, 2-[[6-Amino-3,5-dicyano-4-[4-(cyclopropylmethoxy)phenyl]-2-pyridinyl]thio]-acetamide	Tocris	Cat#4472 CAS#910487-58-0
Adenosine 5′-triphosphate disodium salt hydrate	Sigma-Aldrich	Cat#A7699-1G
VivoGlo Luciferin, In Vivo Grade	Progema	Cat#P1041
IntestiCult^{TM} Organoid Growth Medium	StemCell Technologies	cat# 06005
Matrigel^{TM} Membrane Matrix Growth Factor Reduced	Corning	Cat #354230
Collagenase D	Roche Life Science	cat#11088866001
Critical commercial assays		
CellTiter-Glo Luminescent Cell Viability Assay	Progema	Cat#G7571
RNeasy Mini Kit	Qiagen	Cat#74104
Agilent TapeStation using high sensitivity RNA kit	Agilent	Cat#PN-5067-5579
NEBnext ultra RNA library preparation kit	New England Biolabs Inc	Cat#E7530L
Qubit^{TM} 1× dsDNA High Sensitivity (HS) and Broad Range (BR) Assay Kits	Thermofisher Scientific	Cat#Q33231
NovaSeq Reagent kit - SP flow cells kits	Illumina	Cat#20040326
Deposited data		
NCBI GEO GSE200775	NCBI	GSE200775
Experimental models: Organisms/strains		
B6.129P2-$Lyz2^{tm1(cre)lfo}$/J LysM^{Cre}	The Jackson Laboratory	Jax Strain #**004781**
$Villin^{Cre}$-$A_{2B}AR^{fl/fl}$	Holger K. Eltzschig, University of Texas at Houston Medical School	Aherne et al., 2015
$LysM^{Cre}$-$A_{2B}AR^{fl/fl}$	Holger K. Eltzschig, University of Texas at Houston Medical School	Seo et al., 2015

Continued

REAGENT or RESOURCE	SOURCE	IDENTIFIER
PmeLuc	Di virgilio Francesco, University of Ferrara	Csoka et al., 2018b
CD39$^{-/-}$	Simon C. Robson, Harvard Medical School	Enjyoji et al., 1999
C57BL/6J	The Jackson Laboratory	Jax Strain **#000664**
BALB/c-Il4^{tm2Nnt}/J	The Jackson Laboratory	Jax Strain **#002496**
B6.129P2-Il4^{tm1Cgn}/J IL-4KO mice	The Jackson Laboratory	Jax Strain **#002253**
B6.Cg-Tg(Vil1-cre)997Gum/J Villin^{Cre}	The Jackson Laboratory	Jax Strain **#004586**
BALB/cJ	The Jackson Laboratory	Jax Strain #:**000651**
Oligonucleotides		
Taqman Primer: Interleukin 13	ThermoFisher	Mm99999190_m1
Taqman Primer: Interleukin 33	ThermoFisher	Mm00505403_m1
Taqman Primer: Arg1	ThermoFisher	Mm00475988_m1
Taqman Primer: Retnla	ThermoFisher	Mm00445109_m1
Taqman Primer: Ifng	ThermoFisher	Mm01168134_m1
Taqman Primer: Interleukin 4	ThermoFisher	Mm00445260_m1
Taqman Primer: Interleukin 5	ThermoFisher	Mm00439646_m1
Taqman Primer: Adora2b	ThermoFisher	Mm00839292_m1
Software and algorithms		
SoftMax Pro Software	Molecular Devices	https://www.moleculardevices.com
Living Image Analysis Software	PerkinElmer	https://www.perkinelmer.com Part #128113
LAS Advanced Fluorescence Software	Leica Microsystems	https://www.leica-microsystems.com
Prism Statistical Analysis Software	GraphPad	https://www.graphpad.com
Ingenuity Pathway Analysis (QIAGEN IPA)	Qiagen	https://digitalinsights.qiagen.com/
Image Lab Software	Bio-Rad	https://www.bio-rad.com
CTL Immunospot software	ImmunoSpot	https://immunospot.com

RESOURCE AVAILABILITY

Lead contact
Further information and requests for resources and reagents should be directed to and will be fulfilled by the lead contact, William C. Gause, gausewc@njms.rutgers.edu.

Materials availability
This study did not generate new unique reagents.

Data and code availability
Bulk RNA sequencing data have been deposited at NCBI GEO GSE200775 and are publicly available as of the date of publication. Accession numbers are listed in the key resources table. This paper does not report original code. Any additional information required to access and analyze the data reported in this paper is available from the lead contact upon request.

EXPERIMENTAL MODEL AND SUBJECT DETAILS

8–12-week-old *WT* and *IL-4$^{-/-}$ BALB/c* mice were purchased from The Jackson Laboratory (Bar Harbor, ME). *C57BL/6 WT mice* were purchased from The Jackson Laboratory (Bar Harbor, ME). *Villin^{Cre}-A$_{2B}$AR$^{fl/fl}$* mice (Aherne et al., 2015), *LysM^{Cre}-A$_{2B}$AR$^{fl/fl}$* mice (Seo et al., 2015), *pmeLuc* (Csoka et al., 2018b), *CD39$^{-/-}$* (Enjyoji et al., 1999), *Villin^{Cre}* (Madison et al., 2002), and *LysM^{Cre}* (Clausen et al., 1999) all on a *C57BL/6* background, were bred and housed as previously described. All mice were maintained in a specific pathogen-free, virus Ab-free facility during the experiments. Female and male healthy mice were selected for treatment groups from purchased or bred colonies without using specific randomization methods or specific blinding methods. The studies have been reviewed and approved by the Institutional Animal Care and Use Committee at Rutgers-the State University of New Jersey, and

Columbia University. The experiments herein were conducted according to the principles set forth in the Guide for the Care and Use of Laboratory Animals, Institute of Animal Resources, National Research Council, Department of Health, Education and Welfare (US National Institutes of Health).

METHOD DETAILS

Parasite inoculations

Hpb L3 were isolated from cultures using a modified Baermann apparatus and maintained in PBS at 4°C. To assess memory responses, mice were initially inoculated by oral gavage (per os, p.o.) with 200 infective L3 to establish a primary chronic infection. On days 14 and 15, mice were treated using an anti-helminthic drug (pyrantel pamoate 1mg/mouse) to expulse the parasites. Six weeks post clearance, 200 L3 were administered as a challenge secondary inoculation; naïve control mice were inoculated for a primary infection. Worm burden was determined from the small intestine at day 14 post-primary and challenge infections as described previously (Anthony et al., 2006).

Total ATP assay

Total worm ATP assay was as described previously (Patel et al., 2014). Briefly, for ATP, five female worms were isolated after *Hpb* inoculation of *Villin^{Cre}-A_{2B}AR^{fl/fl}* and *LysM^{Cre}-A_{2B}AR^{fl/fl}* mice and corresponding control *Villin^{Cre}* and *LysM^{Cre}* mice, incubated in 100 μL PBS with 100 μL Cell-Glo reagents (Promega, Madison, WI), and ground with a motorized pestle. After centrifugation at 5,300 rpm for 5 min, 100 μL supernatant was transferred to wells of 96-well plate and luminescence was measured in SpectraMax i3X cytometer. Controls included the following: PBS alone, heat-killed worms; worms incubated without Cell-Glo reagent following manufactures protocol. Absorbance was measured using SpectraMax i3X cytometer as described previously (Patel et al., 2014).

Cytokine gene expression by qPCR

For qPCR, RNA was extracted from the small intestine, MLN, and granuloma punches and reverse transcribed to cDNA using SuperScript II Reverse Transcriptase (Invitrogen, Waltham, MA. qPCR was performed with TaqMan (Applied Biosystems, Waltham, MA) kits and the Applied Biosystems QuantStudio 6 Flex Real-Time PCR System. All data were normalized to 18S ribosomal RNA, and the quantitation of differences between treatment groups was calculated treated/untreated. Gene expression is presented as the fold increase over naïve controls.

Flow cytometry

Mesenteric lymph node cell suspensions were collected and prepared from Hp1', and 2' inoculated *Villin^{cre}* controls and *Villin^{Cre}-A_{2B}AR^{fl/fl}*; washed; blocked with Fc Block; and stained with anti-CD4-APC (RM4-5,), anti-pSTAT6-PE (pY641). Phosphorylation of STAT6 at tyrosine 641 was detected by intracellular staining with PE-conjugated anti-phospho-STAT6 using PhosFlow Fix Buffer I and Perm Buffer III reagents. Peritoneal exudate cell (PEC) suspensions were blocked with Fc Block (BD Biosciences, San Jose, CA, USA) and subsequently stained with specific Abs, including anti-Ly6G FITC, anti-CD11b PerCP/CY5.5, Siglec-F PE, anti-c-kit APC, F4/80 APC, BD Biosciences, San Jose, CA, USA) and anti-CD206PE (Biolegend, USA). Cells were acquired on Fortessa X-20 Flow cytometer (BD Biosciences, San Jose, CA) and analyzed using FlowJo software (Becton Dickinson & Company, Ashland, OR)

Dose and administration of microparticle (MPs)

Cobalt chrome microparticles (MPs) were obtained from Sandvik Osprey Ltd (Neath, Wales, UK). Sterile particles were prepared and redissolved in sterile PBS, as previously described (Mishra et al., 2011). These particles were separated using graded ethanol solution for sedimentation and analyzed by low-angle laser light scattering with a Microtrap X-100 (Bioengineering Solutions, Chicago, IL, USA). MPs ranging from 0.3 to 100μm were used, and a dose of 50mg/mice was given intra-peritoneally for *in vivo* studies in mice.

Adoptive transfers

Adoptive transfers of memory T cells were as previously described (Anthony et al., 2006). Briefly, donor *Villin^{Cre}-A_{2B}AR^{fl/fl}* and corresponding *Villin^{Cre}* control mice were orally inoculated with 200 *Hpb* L3. 14 days later, mice were treated with the anti-helminthic drug, pyrantel pamoate, to expulse the parasites. Six weeks later, mesenteric lymph nodes and spleen single-cell suspensions were used to magnetically sort purify CD4$^+$ T cells using mouse CD4 Microbeads (Miltenyi Biotec, Inc. Auburn, CA). 5×10^6 CD4$^+$ T cells were retro-orbitally injected into sex- and age-matched *Villin^{Cre}-A_{2B}AR^{fl/fl}* naïve recipient mice. Two days after transfer, mice were inoculated with 200 L3 *Hpb*. Mice were harvested 14 days after *Hpb* infection.

CD4$^+$ T cell sorting and ELISPOT

Single-cell suspensions from mesenteric lymph nodes from *Villin^{Cre}-A_{2B}AR^{fl/fl}* and corresponding *Villin^{Cre}* control mice were sort-purified on BD Fusaria II SORP (BD Biosciences, San Jose, CA) by gating on DAPI-, CD4+ T cells. Biological replicates from each group were sorted and purified individually. Two hundred thousand cells/well were seeded on a multiscreen IP filter plate (Millipore Sigma, Burlington, MA) for 24 h. IL-4 ELISPOT was performed using mouse IL-4 ELISPOT pair antibodies (BD Bioscience, San Jose, CA).

Plates were scanned using a CTL C6 Fluorospot Analyzer (Cleveland, OH), and the number of IL-4 secreting CD4 T cells were counted on CTL Immunospot software.

Intestinal epithelial cell dissociation

Single-cell isolation protocols were based on previously published methods (Yu et al., 2018; Haber et al., 2017). Proximal small intestine (10cm) from *Villin^{Cre}*-*A_{2B}AR^{fl/fl}* and control *Villin^{Cre}* mice inoculated with *Hpb* for 24 h were isolated and flushed with ice-cold 1× PBS. Tissue was cut longitudinally and cut into small fragments roughly 2 mm long. Tissue pieces were added to ice-cold isolation buffer (1× HBSS and 20mM EDTA) and shaken at 4°C for 40 mins. After vigorous vortexing, crypts were passed through 100-μm cell strainer and then centrifuged at 200 × g for 10 minutes. Crypts were washed with ice-cold 1× PBS and then centrifuged at 200 × g for 10 minutes. Crypts were dissociated at 37°C for 1 minute in 1× TrypLE and 0.5mg/mL DNAse I. After vigorous vortexing, single-cell suspensions were passed through 70-μm cell strainer and then centrifuged at 200 × g for 10 minutes. Cell pellets were washed with ice-cold 1× PBS and then centrifuged at 200 × g for 10 minutes. Cell pellets were suspended in FACs buffer (1× PBS, 2% FBS, 2% BSA, 2mM EDTA) ready for staining.

Lamina propria cell isolation

Proximal small intestine (10cm) from *Villin^{Cre}*-*A_{2B}AR^{fl/fl}* and control *Villin^{Cre}* mice inoculated with *Hpb* for 24 hours were isolated and flushed with ice-cold 1× HBSS. Tissue was cut longitudinally into small fragments roughly 1-2cm long. Intestinal fragments were incubated in shaking incubator HBSS-1mM DTT at 37°C for 20 min. Intestinal pieces were transferred into HBSS-5mM EDTA buffer and placed into shaking incubator at 37°C for 10–20 minutes until tissue fragments were translucent. Tissue was washed with RPMI and digested in HBSS-Collagenase D (1mg/mL) (Roche Life Science, Penzberg, Germany, catalog#11088866001) buffer for 30 minutes in a shaking incubator at 37°C. Cells were filtered through 70μm cell strainer, washed with RPMI and overlayed in 67% and 44% percoll gradient. Cells in the interface were collected, counted, stained (DAPI, APC- EpCAM, PE-CD45$^+$) and sort-purified on BD FACSAria II SORP (BD Biosciences, San Jose, CA) by gating on DAPI$^-$, EpCAM$^-$, CD45$^+$.

In vivo extracellular ATP measurement

Transgenic plasma-membrane-targeted luciferase (pmeLUC) mice were orally inoculated with 200 L3 *Hpb* or PBS. Twenty-four hours later, 75 mg/kg VivoGlo luciferin (Progema, Madison, WI) in 100uL was injected *i.p.*.10 minutes later; whole body luminometry was performed using the IVIS 200 (Caliper Life Sciences, Hopkinton, MA) preclinical *in vivo* imaging system using Live Image Software (Caliper Life Sciences, Hopkinton, MA) for image capture and ROI measurements, as previously described (Csoka et al., 2018b).

Fluorescent immunohistochemistry and histology

Fresh swiss-rolls of proximal small intestinal tissues (10cm) were embedded in Optimal Cutting Temperature Compound (Tissue-Tek) and flash frozen in 2-Methylbutane/liquid nitrogen and stored at −80°C. 4–5 μm sections were cut on CM1950 Cryostat (Leica, Wetzlar, Germany) and fixed in ice-cold acetone for 8 minutes, blocked with 1% rat serum/1% Fc Block and stained with F4/80-AF488 (clone BM8), CD206-AF647 (5μg/mL), Hoechst 33,342 (2μg/mL) (Invitrogen Waltham, MA catalog #H3570) and sealed with ProLong Gold Antifade (Invitrogen, catalog# P36930,). Fixed tissue staining protocols were adapted from previously published methods (Mcginty et al., 2020; Schneider et al., 2018; Von Moltke et al., 2016). Proximal intestinal tissues (10cm) were flushed with PBS and fixed in 4% paraformaldehyde for 4 hours at 4°C. Tissues were washed with 5mM NH$_4$Cl and incubated in 30% (w/v) sucrose overnight at 4°C. Swiss rolls of fixed duodenum were embedded in Optimal Cutting Temperature Compound (Tissue-Tek), and 8 μm sections were cut on CM1950 Cryostat (Leica, Wetzlar, Germany). Tuft Cell staining: Sections were blocked with 5%goat serum and 1% Fc Block in PBS for 1 hour, followed by primary antibody (α-DCLK1, Abcam catalog# ab31704) for 1 hour, and secondary α-Goat Anti-Rabbit IgG H&L -Alexa Flour (AF)-488 (Abcam, catalog# ab150077), Hoechst 33342 and sealed with ProLong Gold Antifade. Tuft cells were counted manually from the crypt to the villi. Four 20× images were analyzed for each mouse, and at least 30 total villi were counted. Images were taken using a Leica DM6000B fluorescent microscope (Leica Microsystems, Buffalo Grove, IL), Orca Flash 4.0 mounted digital camera (Hamamatsu Photonics K.K., Japan) and LAS Advanced Fluorescence software. Fluorescent channels were photographed separately and then merged. Exposure times and fluorescence intensities were normalized to appropriate control isotype images. IL-33 Staining: Sections were blocked with 5%goat serum and 1% Fc Block in PBS for 1 h, followed by primary antibody Goat Anti-Mouse IL-33 Antigen Affinity-purified Polyclonal Antibody (R&D biosystems Catalog # AF3626) overnight at 4°C, and secondary Donkey anti-Goat, Alexa Fluor 488 (Invitrogen catalog# A11055) and Hoechst 33342 for 1 h. Sealed with ProLong Gold Antifade. Images were captured using a Nikon A1R spectral confocal microscope with GaAsP photodetectors and controlled by Nikon's NIS-Elements software package. The confocal microscope is equipped with a multi-line argon-ion laser (457, 488 and 514 nm), a 561 nm optically pumped semiconductor laser, and a 405 nm and 640 nm laser diode. Nikon Plan Apochromat VC 20×/0.75 and 60×/1.4 oil lenses were used to capture the images. H&E images were taken using a Nikon 50i brightfield microscope, MicroPublisher 6 CCd camera (QImaging, Surrey BC, Canada) and Ocular Scientific Image Acquisition software (QImaging, Surrey BC, Canada). Granulomas' region of interest (ROI) was measured in randomized, blinded methods using three granulomas from each mouse. Granuloma sizes were measured by selecting an ROI and quantitating the area within the granuloma measured in μm^2; three granuloma sections were measured/granuloma separated ten sections apart. ROI determinations were performed by a researcher who did not perform the histological preparations or imaging. Mean ROI measurements were determined for the three sections of

each granuloma, and the mean granuloma value for each mouse was used to determine the mean and standard error for three mice/treatment group.

Bulk RNA sequencing

Villin^{Cre}-A$_{2B}$AR$^{fl/fl}$ and control *Villin^{Cre}* mice were inoculated with *Hpb*, and 24 h later, along with naïve controls, intestinal epithelial cells were sort-purified on BD FACSAria II SORP (BD Biosciences, San Jose, CA) by gating on DAPI$^-$, CD45$^-$, EpCAM$^+$ IECs. Four biological replicates from each group were sorted and purified individually. The purity of cell populations was 98% or greater. Total cellular RNA was extracted using Qiagen RNAeasy (Qiagen Inc, Germantown, MD) protocol according to the manufacturer's instructions. RNA quality was first checked for integrity on an Agilent TapeStation using a high sensitivity RNA kit (Agilent Technologies Inc, CA). Samples with RNA integrity number (RIN) > 7.0 were considered to have sufficient quality for subsequent processing. Illumina compatible cDNA libraries were generated for polyA selected mRNA using NEB next ultra-RNA library preparation kit (New England Biolabs Inc, MA). The cDNA libraries were purified using AmpureXP beads (Beckman Coulter) and analyzed on an Agilent TapeStation (Agilent Technologies Inc, CA) to estimate the size of the library and quantitated using Qubit 4 Fluorometer (Thermofisher Scientific, MA). Equimolar amounts of barcoded libraries pooled together and sequenced on Illumina NovaSeq 6000 Instrument (Illumina, San Diego, CA) using SP flow cells with 2 × 100 cycles configuration. Raw transcriptome reads were assessed for quality control (FASTQC v0.11.8) and trimmed for quality and adapter contaminants (cutadapt v 2.5). Trimmed reads were aligned to the mouse genome (GRCm38) using STAR (v2.6.1), followed by transcript abundance calculation and hit count extraction with StringTie (v2.0) and featureCounts (v1.6.4), respectively. Hit count normalization and differential gene expression group cross-comparisons were performed using DESeq2 (v1.26.0). Significant differentially expressed gene thresholds were set at FDR adjusted p < 0.05. Pathway enrichment was performed using Ingenuity Pathway Analysis (Qiagen Inc, Germantown, MD).

Western blot

Duodenal intestinal tissue was collected from *Hpb* inoculated *Villin^{Cre}-A$_{2B}$AR$^{fl/fl}$* and control *Villin^{Cre}* mice, and 24 h later, along with naïve controls, was lysed in T-PER tissue extraction buffer (Thermo Scientific, Waltham, MA, catalog#78510), with 2× protease inhibitors and 2× EDTA (Thermo Scientific, catalog# 78444). Protein concentration was measured using Bradford protein assay kit (Thermo Scientific, catalog# 23200). 40ug of total protein was loaded to SDS-PAGE gel. Gel was transferred, and PVDF membrane was probed with 0.4 μg/mL of Goat Anti-Mouse IL-33 affinity-purified polyclonal antibody (R&D Biosystems, catalog # AF3626) overnight at 4°C and followed by HRP-conjugated anti-Goat IgG secondary antibody (R&D Biosystems, catalog # HAF109) for 1 h.

Intestinal enteroid generation

Proximal small intestines of *Villin^{Cre}* mice were flushed with ice-cold PBS. Tissue was incubated in 10mL of crypt isolation buffer (1×PBS-2mM EDTA) on a rocker for 5 min at 4°C. Tissue was cut longitudinally into small fragments roughly 0.8cm long and incubated in fresh isolation buffer on a rocker for 45 min at 4°C. After incubation, tubes were shaken vigorously until tissue floated, indicating removal of the mucosal layer. Cell suspensions were passed through 70μm cell strainer. Cells were washed with 1× DMEM and then centrifuged at 50 × g for 10 min. Crypts were counted by hemocytometer and plated at 350 crypts per well in a 1:1 ratio of Matrigel™ Membrane Matrix Growth Factor Reduced (Corning, Cat #354230) to Advanced DMEM/F-12 (Thermo Scientific, catalog #12634-010). Enteroids were cultured for five days in IntestiCult™ Organoid Growth Medium (StemCell Technologies, Vancouver, Canada, catalog # 06005). Wells were treated with 10 μm of BAY 60–6583 (Tocris Bioscience, Bristol, UK, catalog# 4472) or vehicle control (DMSO) for 48 h. Organoids were harvested and lysed in RIPA buffer with 2× protease inhibitors and 2× EDTA (Thermo Scientific, catalog# 78444). Cell lysate protein concentration was determined using Bradford protein assay kit as explained above.

QUANTIFICATION AND STATISTICAL ANALYSIS

Data were analyzed using the statistical program Prism (GraphPad Software, Inc., La Jolla, CA) and reported as means (±SEM). Student's t-test assessed differences between two groups, differences among multiple groups were assessed by one-way ANOVA, and individual two-way comparisons were analyzed using Tukey's multiple comparison test. Differences of p < 0.05 were considered statistically significant.